



**UNIVERSIDADE FEDERAL DE UBERLÂNDIA
FACULDADE DE ENGENHARIA ELÉTRICA
PÓS-GRADUAÇÃO EM ENGENHARIA BIOMÉDICA**

ERIC FERREIRA SCHMIELE

**ENHANCING EEG SPACIAL RESOLUTION USING ESI: A
MOTOR CONTROL STUDY**

UBERLÂNDIA - MG

2019

ERIC FERREIRA SCHMIELE

**ENHANCING EEG SPACIAL RESOLUTION USING ESI: A MOTOR CONTROL
STUDY**

Dissertation presented to the Pós-Graduação em Engenharia Biomédica of the Universidade Federal de Uberlândia, as requirement to obtain the title of Master of Science.

Area of study: Biomedical Engineering
Supervisor: Alcimar Barbosa Soares

UBERLÂNDIA - MG

2019

Ficha Catalográfica Online do Sistema de Bibliotecas da UFU
com dados informados pelo(a) próprio(a) autor(a).

S354 Schmiele, Eric Ferreira, 1993-
2019 ENHANCING EEG SPACIAL RESOLUTION USING ESI: A MOTOR
CONTROL STUDY [recurso eletrônico] / Eric Ferreira Schmiele. -
2019.

Orientador: Alcimar Barbosa Soares.
Dissertação (Mestrado) - Universidade Federal de Uberlândia,
Pós-graduação em Engenharia Biomédica.
Modo de acesso: Internet.
Disponível em: <http://doi.org/10.14393/ufu.di.2020.40>
Inclui bibliografia.
Inclui ilustrações.

1. Engenharia biomédica. I. Soares, Alcimar Barbosa, 1965-,
(Orient.). II. Universidade Federal de Uberlândia. Pós-graduação
em Engenharia Biomédica. III. Título.

CDU: 62:61

Bibliotecários responsáveis pela estrutura de acordo com o AACR2:
Gizele Cristine Nunes do Couto - CRB6/2091
Nelson Marcos Ferreira - CRB6/3074



UNIVERSIDADE FEDERAL DE UBERLÂNDIA

Coordenação do Programa de Pós-Graduação em Engenharia Biomédica
Av. João Naves de Ávila, 2121, Bloco 3N, Sala 115 - Bairro Santa Mônica, Uberlândia-MG, CEP 38400-902
Telefone: (34) 3239-4761 - www.ppgeb.feelt.ufu.br - ppegb@feelt.ufu.br



ATA DE DEFESA - PÓS-GRADUAÇÃO

Programa de Pós-Graduação em:	Engenharia Biomédica			
Defesa de:	Dissertação de Mestrado Acadêmico, 054, PPGEB			
Data:	dezoito de dezembro de dois mil e dezenove	Hora de início:	14:15 horas	Hora de encerramento:
Matrícula do Discente:	11712EBI008			
Nome do Discente:	Eric Ferreira Schimiele			
Título do Trabalho:	Enhancing EEG's Spacial Resolution Using ESI: A Motor Control Study			
Área de concentração:	Engenharia Biomédica			
Linha de pesquisa:	Engenharia de Reabilitação e Tecnologias Assistivas			
Projeto de Pesquisa de vinculação:	Integração Sensório-Motora e Cognitiva: Modelos Para Potencialização do Reaprendizado Motor de Pacientes Paréticos Pós-AVE			

Reuniu-se no sala de reuniões do LTAD (FEMEC), Campus Santa Mônica, da Universidade Federal de Uberlândia, a Banca Examinadora, designada pelo Colegiado do Programa de Pós-graduação em Engenharia Biomédica, composta pelos professores doutores: João Batista Destro Filho - FEELT/UFU; Leonardo Abdala Elias - UNICAMP; Alcimar Barbosa Soares - FEELT/UFU orientador do candidato.

Iniciando os trabalhos o presidente da mesa, Prof. Alcimar Barbosa Soares, apresentou a Comissão Examinadora e o candidato, agradeceu a presença do público, e concedeu ao Discente a palavra para a exposição do seu trabalho. A duração da apresentação do Discente e o tempo de arguição e resposta foram conforme as normas do Programa.

A seguir, o senhor presidente concedeu a palavra, pela ordem sucessivamente, aos examinadores, que passaram a arguir o candidato. Ultimada a arguição, que se desenvolveu dentro dos termos regimentais, a Banca, em sessão secreta, atribuiu o resultado final, considerando o candidato

Aprovado.

Esta defesa faz parte dos requisitos necessários à obtenção do título de Mestre.

O competente diploma será expedido após cumprimento dos demais requisitos, conforme as normas do Programa, a legislação pertinente e a regulamentação interna da UFU.

Nada mais havendo a tratar foram encerrados os trabalhos. Foi lavrada a presente ata que após lida e achada conforme foi assinada pela Banca Examinadora.



Documento assinado eletronicamente por **Alcimar Barbosa Soares, Professor(a) do Magistério Superior**, em 18/12/2019, às 18:09, conforme horário oficial de Brasília, com fundamento no art. 6º, § 1º, do [Decreto nº 8.539, de 8 de outubro de 2015](#).



Documento assinado eletronicamente por **Leonardo Abdala Elias, Usuário Externo**, em 18/12/2019, às 19:00, conforme horário oficial de Brasília, com fundamento no art. 6º, § 1º, do [Decreto nº 8.539, de 8 de outubro de 2015](#).



Documento assinado eletronicamente por **João Batista Destro Filho, Professor(a) do Magistério Superior**, em 19/12/2019, às 11:35, conforme horário oficial de Brasília, com fundamento no art. 6º, § 1º, do [Decreto nº 8.539, de 8 de outubro de 2015](#).



A autenticidade deste documento pode ser conferida no site
https://www.sei.ufu.br/sei/controlador_externo.php?acao=documento_conferir&id_orgao_acesso_externo=0, informando o código verificador **1772467** e o código CRC **6FFBA270**.

I dedicate this work to my mother.

ACKNOWLEDGEMENTS

I thank God for giving me the opportunity of having this journey and for helping me so much during it even through all hardships. He is the reason why I'm living, and He is the reason why I'll continue to live.

I thank my family, specially my mother, Késia Ferreira, for all the support love and care she has given me in all aspects of life even though being distant. I should also specially mention my uncles Sérgio Ferreira, Oscar Simonetti and my aunt Jussara Ferreira Simonetti for helping me during my life changes and for supporting my mom when I wasn't able to. They all helped me regardless of difficulty and I hope I can retrieve the favour in the future.

I thank my supervisor, Alcimar Barbosa Soares, for all the helping he has given me and all the wisdom he shared with me, not to mention the patience he demonstrated during this whole endeavour.

I thank my girlfriend, Débora Amorim, for giving me great psychological support and for providing a great impetus for finishing this whole project and to keep looking forward.

I thank my psychologist, Fábio Alves dos Reis, for helping me persevere through this journey and for listening to my problems as well as helping me to understand them and to solve them.

I thank BioLab and all my colleagues from it who helped in decisions and calculations, not to mention the good times we shared during our academical journeys.

I also thank the funding agency, CAPES, for making this whole research possible and for aiding so many other projects at BioLab.

“I have not failed.
I’ve just found 10,000 ways that won’t work.”

Thomas Edison

ABSTRACT

Though electroencephalography (EEG) signals have been widely used to extract brain information they have a low spatial resolution and are not as capable as invasive techniques for applications which demand more specific information from the brain, which would highly enhance the power of brain machine interfaces (BMIs). Because of that, there is a great interest in enhancing EEG's spatial resolution using electromagnetic source imaging (ESI), which combines EEG signals and magnetic resonance images (MRI) to reconstruct the brain's internal current sources (CSs). To investigate the level of information enhancement that ESI can achieve, we proposed to investigate the brain activity differences in signal behavior and position during different movements from the same limb. To do that we applied ESI to simulated data for initial validation, reaching an average correlation coefficient of 0.99 and an average physical displacement of 15.0 mm comparing simulated and calculated signals. Then we applied ESI to EEG recordings of hand, wrist and elbow movements and compared the source signals to the expected neural behavior known from the literature. Thanks to ESI, we reconstructed more than 8000 source points from a total of 61 electrodes enhancing the resolution from an average of 24.69 mm to 3.67 mm. Thanks to this enhancement we were able to analyze spatial and time-frequency information which correlated with the performed movements in accordance to the literature. Therefore, we showed the potential of ESI for applications that demand a better interpretation of brain signals in questions of control of different movements from a single limb.

Keywords: *Electroencephalography, spatial resolution, Electromagnetic Source Imaging, motion control, single limb.*

CONTENTS

Abstract	viii
List of Figures	xii
List of Tables	xvi
List of Abbreviations	xvii
1 Introduction	1
1.1 Motivation	1
1.1.1 Basic outline	5
1.2 Objectives	5
1.2.1 General Objective	5
1.2.2 Specific Objectives	5
2 Brain signals and motor control	6
2.1 Basic brain anatomy and physiology	6
2.2 Brain motor control	7
2.2.1 Premotor cortex	8
2.2.2 Primary motor cortex	8
2.2.3 Primary somatosensory cortex	9
2.3 Electroencephalography signals	10
2.3.1 Interpreting EEG signals related to movement	11
2.3.2 EEG limitation	12
3 Electromagnetic Source Imaging	14
3.1 Applications	15

3.2	Main equation	15
3.3	Forward problem	16
3.3.1	Concentric spheres	16
3.3.2	Boundary element method	17
3.3.3	Finite element method	17
3.3.4	Lead field matrix	18
3.4	Inverse problem	19
3.4.1	Minimal norm estimate	19
3.4.2	sLORETA	20
3.4.3	eLORETA	20
3.5	Data analysis	21
3.5.1	Sources of interest	21
3.5.2	Recalculated average direction	22
4	Methodology	23
4.1	Lead field calculation	23
4.2	Validation with simulated signals	24
4.2.1	Signal generation	25
4.2.2	Comparison metrics	26
4.2.2.1	Correlation coefficient	26
4.2.2.2	Distance between main sources	27
4.2.3	Further validation	27
4.3	Application with real data	27
4.3.1	Data set	28
4.3.2	EEG preprocessing	29
4.3.3	ESI calculation	30
4.3.3.1	Regularization parameter	30
4.3.4	Region of interest	31
4.3.5	Dimension reduction	31

4.3.6	ESI analysis	32
5	Results and Discussions	34
5.1	Stage 1: Validation using simulated data	34
5.2	Stage 2: Application using real EEG signals	39
5.2.1	Regularization parameter	39
5.2.2	CS power and RAD analysis	40
5.2.3	Main related CSs	45
6	Conclusion	53
6.1	Future works	54
Bibliography		54

LIST OF FIGURES

1.1	Motor and somatosensory cortices highlighting areas mostly related to face (green), hand (fingers and palm) (blue) and other regions such as forearm, elbow, shoulder, trunk, legs and so on (yellow).	2
1.2	(a) Brain regions mostly related to movements: ventral premotor cortex (yellow); dorsal premotor cortex (blue); primary motor cortex (green); and primary somatosensory cortex (red).; (b, c and d) projection of EEG electrodes directly over the specified regions considering different electrode distributions (10/20, 10/10 and 10/05 respectively).	3
2.1	Basic brain regions (adapted from: Purves <i>et al.</i> (2004)).	6
2.2	Brain regions related to motor control: PM (blue), M1 (red) and S1 (green).	7
2.3	Left hemisphere's dPM (blue) and vPM (yellow).	8
2.4	Sections along the primary motor cortex and the somatosensory cortex highlighting the body regions most related to its subdivisions (adapted from: Purves <i>et al.</i> (2004)).	9
2.5	EEG electrode locations according to the 10/10 system (64 electrodes).	10
2.6	Cellular composition of the grey matter, including the pyramidal cell layer (adapted from: Purves <i>et al.</i> (2004)).	11
2.7	(a) Brain regions mostly related to movements: ventral premotor cortex (yellow); dorsal premotor cortex (blue); primary motor cortex (green); and primary somatosensory cortex (red).; (b, c and d) projection of EEG electrodes directly over the specified regions considering different electrode distributions (10/20, 10/10 and 10/05 respectively).	13
3.1	CS distribution for a given head model with more than 8000 CSs.	14
3.2	Concentric sphere model (adapted from: JAIR MONTOYA MARTÍNEZ (2014)).	17
3.3	BEM model (adapted from: JAIR MONTOYA MARTÍNEZ (2014)).	18
3.4	FEM model (adapted from: JAIR MONTOYA MARTÍNEZ (2014)).	18

4.1	Used electrode and source positions.	24
4.2	(a, b and c) CSs chosen for the simulations with 1, 3 and 10 main CSs respectively.	25
4.3	Example of simulated signals for each direction of one CS.	26
4.4	EEG channels used for data collection.	28
4.5	EEG ICA decomposition and eliminated components through correlation with EOG (red) and visual analysis (magenta).	29
4.6	Example of window from EEG channel C3 and the exoskeleton elbow signal (normalized) used to determine the movement onset.	30
4.7	Brain ROIs separated for dimension reduction: vPM (yellow); dPM (blue); upper half from the M1 (green); and upper half from the S1 (red).	32
4.8	Electrodes used in the data set acquisition and CSs found right above and inside the ROI (respectively).	32
5.1	Simulation using 1 main CS. (a) power from the main CS and a cursor indicating the time sample for the following subfigures; (b and c) CS power in a specific time sample from the simulated and calculated source spaces respectively.	35
5.2	Simulation using 3 main CSs. (a) power from the main CSs and a cursor indicating the time sample for the following subfigures; (b and c) CS power in a specific time sample from the simulated and calculated source spaces respectively.	36
5.3	Simulation using 10 main CSs. (a) power from the main CS and a cursor indicating the time sample for the following subfigures; (b and c) CS power in a specific time sample from the simulated and calculated source spaces respectively.	37
5.4	Source space calculation and recalculation using real EEG data. (a) shows the CSs calculated from a real EEG signal. (b) shows the CSs recalculated from an EEG which was calculated from (a).	39
5.5	Convergence from the genetic algorithm for finding the best gene (λ) value by finding the minimal score (error) value.	40
5.6	CS's RAD and power levels from the onset instant for different hand opening movements for a single subject. (a,b,c) Power levels; (d,e,f) RAD values.	41

5.7	CS's RAD and power levels from the onset instant for different hand closing movements for a single subject. (a,b,c) Power levels; (d,e,f) RAD values.	41
5.8	CS's RAD and power levels from the onset instant for different wrist supination movements for a single subject. (a,b,c) Power levels; (d,e,f) RAD values.	42
5.9	CS's RAD and power levels from the onset instant for different wrist pronation movements for a single subject. (a,b,c) Power levels; (d,e,f) RAD values.	42
5.10	CS's RAD and power levels from the onset instant for different elbow extension movements for a single subject. (a,b,c) Power levels; (d,e,f) RAD values.	43
5.11	CS's RAD and power levels from the onset instant for different elbow flexion movements for a single subject. (a,b,c) Power levels; (d,e,f) RAD values.	43
5.12	CS power levels and EEG topographic analysis during different movements for a single subject in a continuous segment. (a) Limb positions from data glove and exoskeleton for wrist (blue), hand (red) and elbow (yellow) movement and a cursor (green) indicating the time sample for each of the following sub-figures respectively; (b, c and d) EEG topographic analysis during wrist, hand and elbow movements respectively; (e, f and g) CS power levels during wrist hand and elbow movements respectively.	46
5.13	CSs from the ROI considered as most relevant for hand movement (between before and during motor planning: a; and between motor planning and execution: b). Point colors indicate the level of <i>mu</i> power difference for each CS.	47
5.14	CSs considered for time and frequency analysis in magenta. Surface colors indicate brain sub-regions: vPM (yellow); dPM (blue); M1 (green); and S1 (red).	47
5.15	Limb positions during hand movement from subject 1 presented along with the spectrogram of the five specific CSs considered as relevant. Color values are from dark blue (lowest) to dark red (highest).	48
5.16	Limb positions during wrist movement from subject 1 presented along with the spectrogram of the five specific CSs considered as relevant. Color values are from dark blue (lowest) to dark red (highest).	48

5.17	Limb positions during elbow movement from subject 1 presented along with the spectrogram of the five specific CSs considered as relevant. Color values are from dark blue (lowest) to dark red (highest).	49
5.18	Limb positions during hand opening and closing movements from subject 1 presented along with the spectrogram of the five specific CSs considered as relevant presented from top to bottom (CS1 to CS5). Color values are from dark blue (lowest) to dark red (highest). . . .	50
5.19	Limb positions during wrist supination and pronation movements from subject 1 presented along with the spectrogram of the five specific CSs considered as relevant presented from top to bottom (CS1 to CS5). Color values are from dark blue (lowest) to dark red (highest).	51
5.20	Limb positions during elbow extension and flexion movements from subject 1 presented along with the spectrogram of the five specific CSs considered as relevant presented from top to bottom (CS1 to CS5). Color values are from dark blue (lowest) to dark red (highest).	52

LIST OF TABLES

4.1	Number of sources and their general positions for each CS simulation.	25
5.1	Total CC, Focal CC, and specific point distance between simulated and calculated sources in all cases (1, 3 and 10 focal points) for the eLORETA method.	34
5.2	Total CC, Focal CC, and specific point distance between simulated and calculated sources in all cases (1, 3 and 10 focal points) for the sLORETA method.	38
5.3	Total CC, Focal CC, and specific point distance between simulated and calculated sources in all cases (1, 3 and 10 focal points) for the MNE method.	38
5.4	Averages of Total CC, Focal CC, and specific point distance between simulated and calculated sources having 10 random sources activated for the MNE, sLORETA and eLORETA methods.	38
5.5	Total CC, Focal CC, and specific point distance between simulated and calculated sources in real data for the eLORETA method.	39

LIST OF ABBREVIATIONS

EEG Electroencephalogram

BMI Brain machine interface

ESI Electromagnetic source imaging

MRI Magnetic resonance image

CS Current source

ECoG Electrocorticogram

LFP Local field potential

fMRI Functional magnetic resonance image

PM Premotor cortex

M1 Primary motor cortex

S1 Primary somatosensory cortex

dPM Dorsal premotor cortex

vPM Ventral premotor cortex

SMA Supplementary motor area

ERS Event related synchronization

ERD Event related desynchronization

BEM Boundary element method

FEM Finite element method

MNE Minimal norm estimate

sLORETA Standardized low resolution brain electromagnetic tomography

eLORETA Exact low resolution brain electromagnetic tomography

RAD Refined average direction

PCA Principal component analysis

SNR Signal to noise ratio

CC Correlation coefficient

EOG Electrooculogram

ICA Independent component analysis

ROI Region of interest

1 INTRODUCTION

1.1 Motivation

In the past decade, many different techniques have provided us with better understanding of the brain as a whole. From sensory-motor control to feelings or even brain connectivity, we are each day learning more about the organ which coordinates ourselves. We have reached the point of brain machine interfaces (BMIs) which allow people to interact with the world in a new way or to regain, to a certain extent, a previously lost way of interaction (NICOLAS-ALONSO; GOMEZ-GIL, 2012).

One of these ways of interaction is motion. Mainly, upper limb motion. Studies on upper limb prosthesis are of utmost importance since their application can help the injured person to perform multiple day-by-day tasks and even help them on their psychological and social reintegration (CORDELLA *et al.*, 2016).

However, since the majority of studies on prosthesis rely on electromyographic signals, they depend highly on the quality of the nerve endings of the lost limb, making some subjects unable to use them correctly (CORDELLA *et al.*, 2016).

Fortunately, and thanks to the last scientific advances we have a better understanding of how the brain controls our movements. Therefore, the next step would be gathering this motor control knowledge, apply it on a BMI and use it to control a prosthesis or orthosis. This goal is already being pursued by many teams through many different approaches and techniques (KAO *et al.*, 2015; BLEICHNER *et al.*, 2014; JERBI *et al.*, 2011; LEEB *et al.*, 2015; LOTTE *et al.*, 2007; NAM; KIM, 2017; SHAKEEL *et al.*, 2015; Udhaya Kumar; Hannah Inbarani, 2017; WODLINGER *et al.*, 2015a). However, there are some obstacles to overcome. For instance, the level of information that can be acquired from the brain in terms of spatial resolution. The brain motor control regions for different parts of the same limb are very close to each other (TAYLOR, 1950; KOCAK *et al.*, 2009). Figure 1.1 shows the motor control and sensory regions for face, hand and other body parts. Therefore, a high spatial resolution is required in order to better differentiate between different motions from the same limb (VALYEAR; FREY, 2015; SEDOV *et al.*, 2016; LEO *et al.*, 2016).

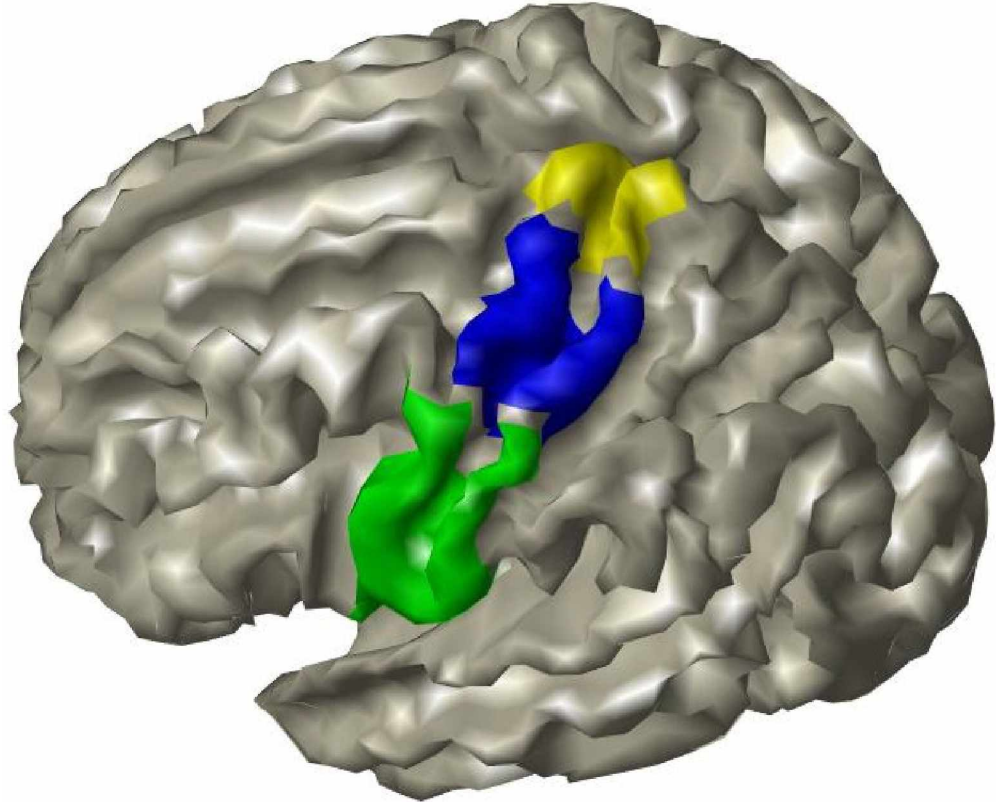


Figure 1.1: Motor and somatosensory cortices highlighting areas mostly related to face (green), hand (fingers and palm) (blue) and other regions such as forearm, elbow, shoulder, trunk, legs and so on (yellow).

Knowing this, it is understandable that Electroencephalography (EEG), one of the most known and used technique for sampling brain information, becomes limited. EEG can have up to 0.05 s and 10 mm of temporal and spatial resolution respectively (NICOLAS-ALONSO; GOMEZ-GIL, 2012) using a 10/05 electrode placement system, with 200 electrodes. However, this only grants up to 16 electrodes over motor control regions of interest for upper limb control, as shown in Figure 1.2. Figure 1.2 also shows that for a 10/20 electrode placement system, this electrode distribution decreases to only 1 electrode above the upper limb control regions. Therefore, many EEG based BMIs can only differentiate between movements of different limbs or final postures of a given limb (SHAKEEL *et al.*, 2015; Udhaya Kumar; Hannah Inbarani, 2017; LEEB *et al.*, 2015; LOTTE *et al.*, 2007) and grant very few dynamical information about the motion (JERBI *et al.*, 2011), only if it is or is not being executed.

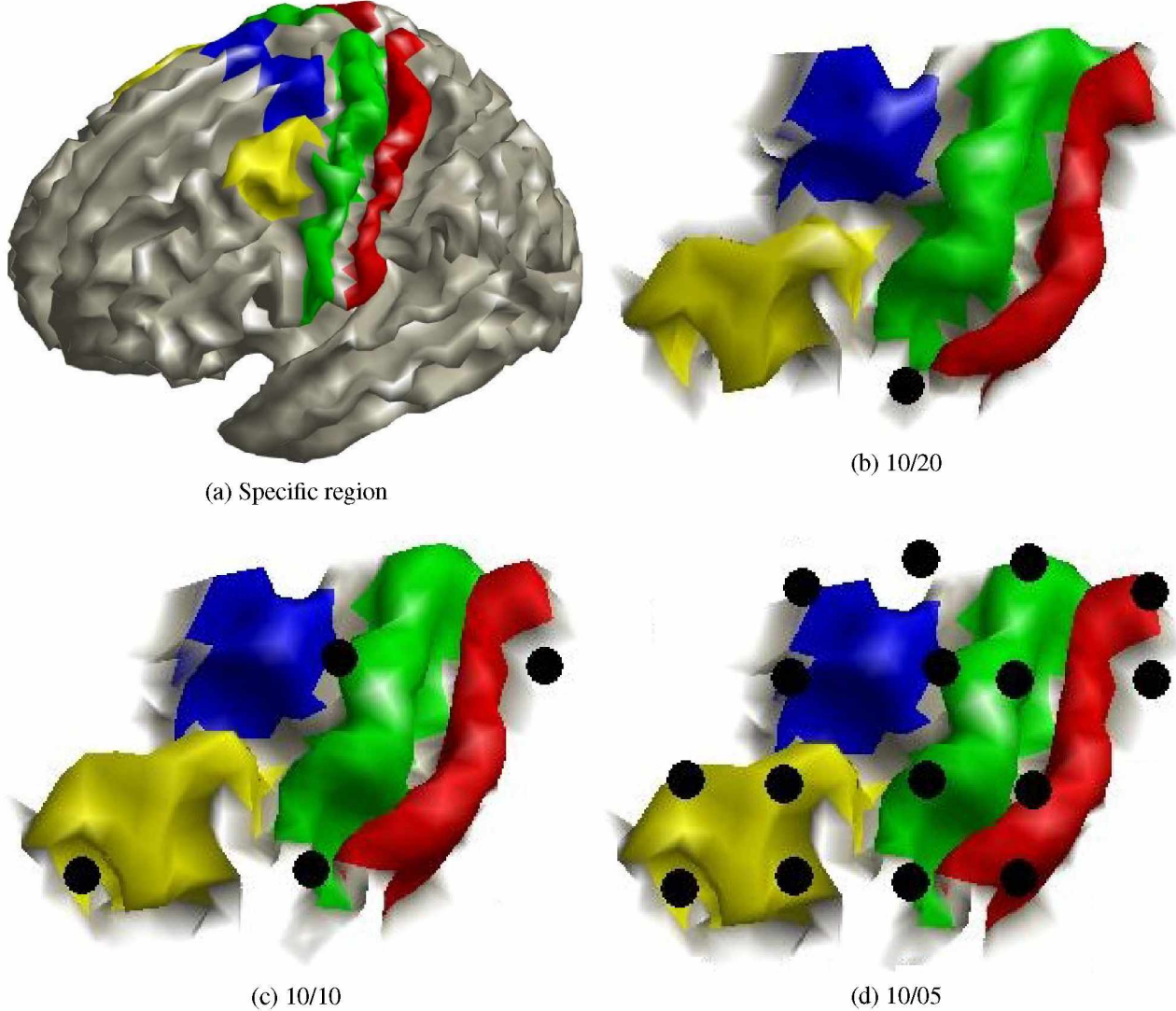


Figure 1.2: (a) Brain regions mostly related to movements: ventral premotor cortex (yellow); dorsal premotor cortex (blue); primary motor cortex (green); and primary somatosensory cortex (red).; (b, c and d) projection of EEG electrodes directly over the specified regions considering different electrode distributions (10/20, 10/10 and 10/05 respectively).

The best techniques to retrieve dynamical information are invasive, such as electrocorticography (ECoG) and local field potentials (LFPs) with around 0.05 s and 1 mm of temporal and spacial resolutions respectively (NICOLAS-ALONSO; GOMEZ-GIL, 2012). These techniques use electrodes very close to the regions of interest, and have an increase in signal to noise ratio given that the acquired signals did not pass through skull or scalp tissue, and have even been used for dynamical movement analysis (WODLINGER *et al.*, 2015b; BUNDY *et al.*, 2016; RANADE;

GANGULY; CARMENA, 2009). However, they are invasive techniques none the less, requiring a delicate surgical procedure which might bring some inconvenience to the patient. Moreover, the used internal electrodes are susceptible to degradation or isolation through the body's immune response (GUNASEKERA *et al.*, 2015), giving it a limited time of optimal functionality.

Fortunately, there is a technique which increases EEG's spatial resolution using MRI, having the same temporal resolution of an EEG and a spatial resolution comparable to the MRI (MICHEL *et al.*, 2004; GRECH *et al.*, 2008; JATOI *et al.*, 2014). Electromagnetic source imaging (ESI) calculates the inner brain current sources (CSs) using EEG signals, a head model, usually acquired from an MRI image and a mathematical method. There is a great range of ESI methods, which are already being applied in studies in the areas of: locating epileptic focal points (BRODBECK *et al.*, 2009; VULLIEMOZ *et al.*, 2010; CUSTO *et al.*, 2014; COITO *et al.*, 2016); connectivity analysis (HASSAN *et al.*, 2014; COITO *et al.*, 2016; MAHJOORY *et al.*, 2017); and even BMIs (HAUFE *et al.*, 2011; EDELMAN; BAXTER; HE, 2015; EDELMAN; BAXTER; HE, 2016; YOSHIMURA *et al.*, 2017).

Yet, though ESI can enhance the spatial resolution of the EEG signal it is important to investigate to what extent we can correctly analyze phenomena from more specific and close internal brain regions. For example, we can find differences between hand and elbow movements, considering that the brain regions related to them are very close (PURVES *et al.*, 2004), as shown in figs. 1.1 and 1.2.

In order to differentiate between movements from the hand, wrist and elbow, it would be necessary to read each different sub-region from the primary motor cortex (M1) (VALYEAR; FREY, 2015). Each of these sub-regions are believed to be encode many different information from the movement (direction, velocity, etc.) (BALL *et al.*, 1999; NAKANISHI *et al.*, 2017), which, would allow for a better movement differentiation. This would require signals with a higher spatial resolution.

Since ESI has already been vastly used for finding focal points of epilepsies, then it might be able to reconstruct CSs from locations as close as the ones responsible for hand, wrist and elbow movement. Therefore, we hypothesize that the use of ESI might provide better localization of information during movements from different parts of the same limb, allowing for a better

differentiation between those, and even for a deep analysis of the regions and signals related to the movement. If such is true, then ESI might be applicable for BMI as well as other studies.

1.1.1 Basic outline

In order to prove our hypothesis we separated the whole process into two main stages: (1) Validation, where we applied the chosen ESI method to simulated data and verified its performance; and (2) Application, where we applied the ESI method to a previously sampled EEG data set from 15 subjects performing hand, wrist and elbow movements, in order to verify the reliability of information granted using ESI.

1.2 Objectives

1.2.1 General Objective

We intend to find a reliable increase of information using ESI on EEG to the point of verifying a significant and consistent difference on signals in close brain regions during three distinct limb movements akin to the ones already established in the literature.

1.2.2 Specific Objectives

The specific objectives are:

- To chose an applicable ESI method using simulated data;
- To validate the chosen ESI method using real data;
- To verify that the ESI calculated signals from real data are in accordance to the expected general brain knowledge;
- To find a good metric to locate the most relevant CSs for a specific activity;
- To analyse the signals from the relevant CSs in time and frequency domains in order to find significant differences between activities that correlate to literature knowledge.

2 BRAIN SIGNALS AND MOTOR CONTROL

In order to better understand this whole study it is necessary to first explain a few basic and specific details about the brain, as well as the EEG recording and application in the field of motor control BMIs.

2.1 Basic brain anatomy and physiology

The brain is comprised of many neurons, about 10^{10} only in its outer layer, which can also be different among themselves. These are cells which send information to and from the brain. Since they can have many types, shapes and sizes they are responsible for our thoughts, feelings, sensations, decisions and memories.

The arrangement of these neurons, along with other brain cells, give rise to several different structures inside the brain with their own purposes. Because of that, there are many different ways to subdivide the brain. One of the most basic ones is the separation between two bigger outer/higher regions: the cerebrum and the cerebellum; and other inner/deeper regions such as diencephalon, midbrain, pons and medulla, all shown in Figure 2.1 (PURVES *et al.*, 2004).

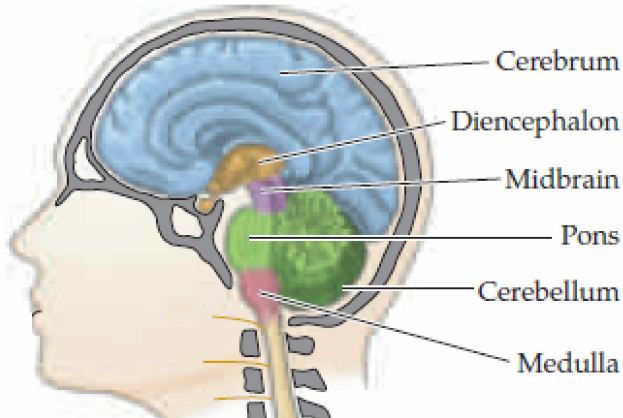


Figure 2.1: Basic brain regions (adapted from: Purves *et al.* (2004)).

2.2 Brain motor control

For a long time, many studies have investigated how the brain controls voluntary movement, and while there are still many unanswered questions, we certainly have a better understanding about brain regions related to movement planning and control. And though many brain regions have some influence on movement control there are a few from the outer layer of the cerebrum which are most studied (MAYHEW *et al.*, 2017): premotor cortex (PM), primary motor cortex (M1), and primary somatosensory cortex (S1), which are shown in Figure 2.2.

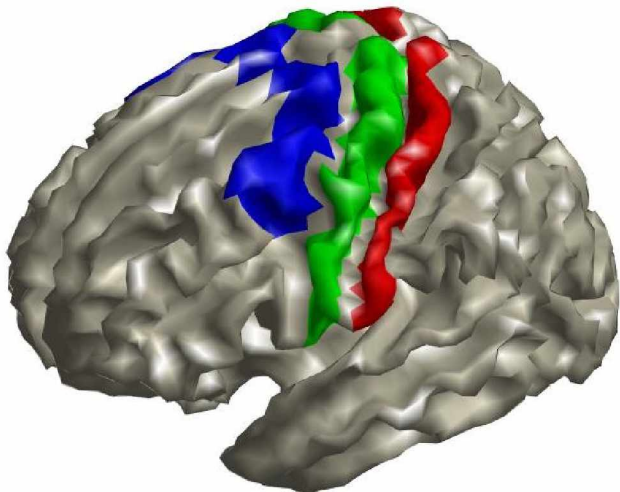


Figure 2.2: Brain regions related to motor control: PM (blue), M1 (red) and S1 (green).

Though, the brain consists not only of the superficial gray matter region (cerebrum's surface) and there are many other deeper brain regions related to the whole motor control process, like the basal ganglia and the cerebellum (HASLINGER *et al.*, 2002; GERARDIN *et al.*, 2004), these are still connected to the aforementioned regions within a series of closed loops. Therefore, the influence of these deeper regions might be determined through changes in the higher regions (MIDDLETON; STRICK, 2000; GERARDIN *et al.*, 2004; KATO *et al.*, 2015).

With that knowledge, we should further understand the role of each higher brain region related to intentional motor control. Here on-wards we will discuss about brain activities during specific movement instants: movement onset, which is when the muscles start contraction; movement planning, which begins from 0.2 to 0.5 s before movement onset; and movement control and

execution, which happens from movement onset to movement completion which will be considered as when the limb gets to a static position.

2.2.1 Premotor cortex

PM is usually related to movement planning, it is where the brain decides which movement should be done by which limb and some other dynamic information for its performance (BALL *et al.*, 1999; VALYEAR; FREY, 2015). It can be further divided into dorsal and ventral PM's (dPM and vPM), shown in Figure 2.3. Furthermore in the upper region of the dPM there is the supplementary motor area (SMA) which is known to be highly related to planning of voluntary movements (TAYLOR, 1950; HASLINGER *et al.*, 2002) and may even have sub-regions within it related to different movement stages (LEE; CHANG; ROH, 1999).

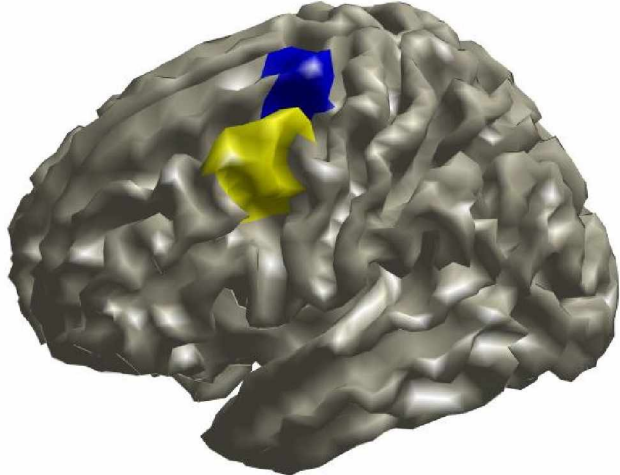


Figure 2.3: Left hemisphere's dPM (blue) and vPM (yellow).

2.2.2 Primary motor cortex

The M1 is the region most directly responsible for movement activation as the primary motor neurons descend from it. These neurons descend to the spinal cord where they send their signals to the lower motor neurons which are connected to the muscles (PURVES *et al.*, 2004).

The M1 is usually divided into sub-regions related to different body parts (PURVES *et al.*, 2004), as represented in Figure 2.4. Though it has already been pointed out that these are not totally

separated from each other as there are interconnections between them (SANTELLO *et al.*, 2016; THOMAS *et al.*, 2019), these regions give a good initial idea of which signals to investigate given that the limb and movement of interest are known.

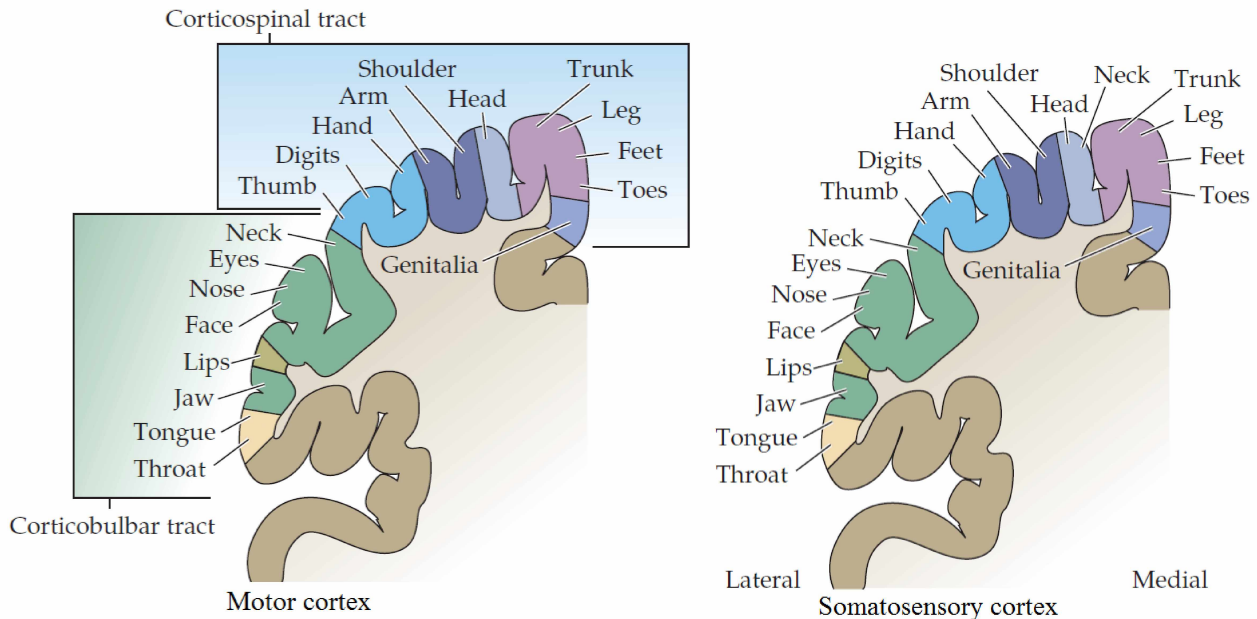


Figure 2.4: Sections along the primary motor cortex and the somatosensory cortex highlighting the body regions most related to its subdivisions (adapted from: Purves *et al.* (2004)).

2.2.3 Primary somatosensory cortex

S1 is related to the main touch senses of the body as well as proprioception from each limb and joint. Like M1, it is also divided into sub regions mostly related to a specific limb (PURVES *et al.*, 2004; THOMAS *et al.*, 2019), as shown in Figure 2.4.

Though this cortex is not directly related to movement, it has a great influence since it grants information from the external environment, which might require the movement to be slightly altered in order to adapt to such information. This alteration might include a difference in direction or strength for example. Therefore, S1 is highly related to motion control for giving it feedback about the performed actions (BALL *et al.*, 1999; VALYEAR; FREY, 2015; MAYHEW *et al.*, 2017). Moreover, these connections are not only related to the main motor region M1, but also to the planning regions dPM and vPM (HASLINGER *et al.*, 2002).

2.3 Electroencephalography signals

One of the most used techniques for brain signal acquisition, EEG signals are electric signals sampled from surface electrodes placed on the scalp of a subject, as illustrated in Figure 2.5. These signals are generated from electrical activities inside the brain and grant valuable information from said activities.

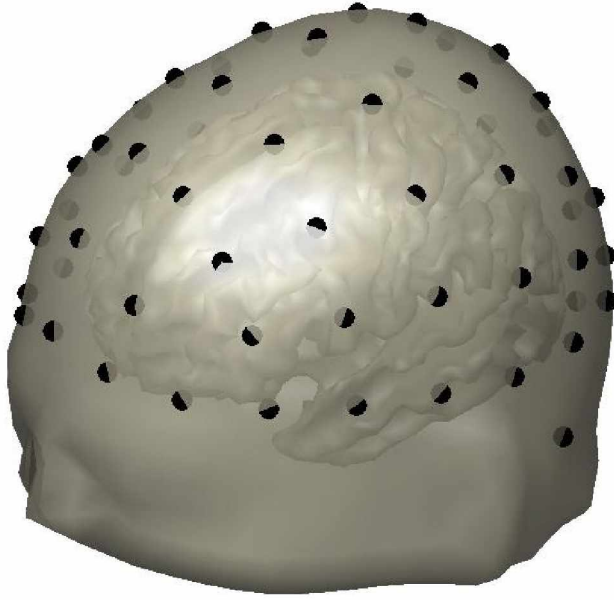


Figure 2.5: EEG electrode locations according to the 10/10 system (64 electrodes).

The electrical signals acquired by the EEG are the result of various electrical fields generated by electrical dipoles inside the brain (HÄMÄLÄINEN *et al.*, 1993). Though each neuron is a possible dipole, considering the size of each neuron and their dipole orientation, it is safe to say that the majority of signals sampled in the EEG originate from the pyramidal neurons (HÄMÄLÄINEN *et al.*, 1993; HALLEZ *et al.*, 2007), shown in Figure 2.6. These neurons are bigger than others around them, closer to the brain surface and are perpendicular to it, therefore, they are the neurons with the biggest influence on the signals once many other neurons generate dipoles with spread orientations that end up cancelling each other (HÄMÄLÄINEN *et al.*, 1993; HALLEZ *et al.*, 2007).

Once the electrical fields generated by the neuron dipoles spread to all dimensions, every EEG electrode will be influenced by every dipole considering their initial amplitude, direction, position and the conductivity of the body tissue between them and the electrodes. Therefore, the signal

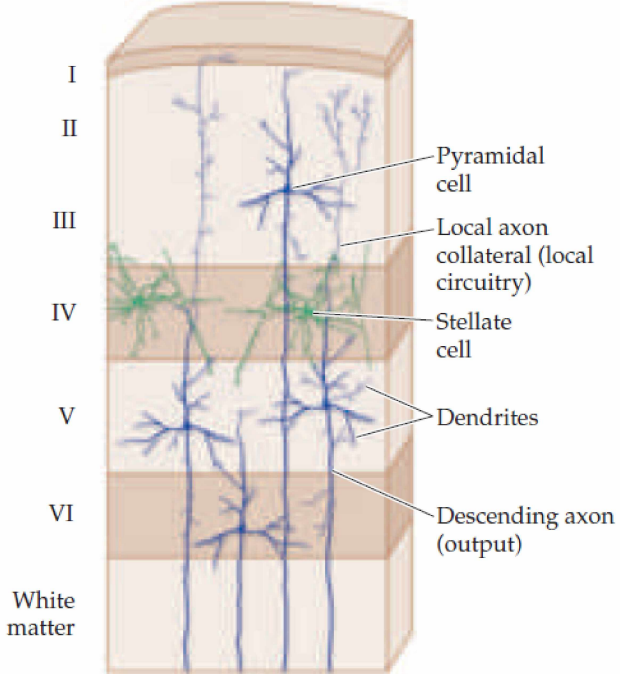


Figure 2.6: Cellular composition of the grey matter, including the pyramidal cell layer (adapted from: Purves *et al.* (2004)).

from one electrode will be strongly influenced by the brain dipoles closest to them (HÄMÄLÄINEN *et al.*, 1993).

2.3.1 Interpreting EEG signals related to movement

The signals that are formed in the EEG electrodes can be interpreted through visual or computational analysis. These take into account different signal characteristics from the time and frequency domain, the later which is highly used in cases considering signals related to movement control.

During movement there is a high event related synchronization (ERS) in the *beta* frequency rhythm (12 to 32 Hz) and a high event related desynchronization (ERD) in the *mu* frequency rhythm (8 to 12 Hz) (NICOLAS-ALONSO; GOMEZ-GIL, 2012). These ERS and ERD are strongly related and can be seen as an increase and a decrease in the power values for these frequency rhythms respectively. Usually, *mu* ERD starts before the movement onset and reaches its maximum shortly after it, while *beta* ERS starts right after movement onset and reaches its maximum after movement execution (NICOLAS-ALONSO; GOMEZ-GIL, 2012).

Furthermore, there can even be more information encoded in these signal characteristics. Boonstra *et al.* (2007) have evidenced that *beta* rhythms also change given motor learning and whether the movement was single or repetitive.

Yet, the original signals can grant even more information, since studies using ECoG and LFP show that there is even more information, such as movement trajectory, in low frequency rhythms such as *mu* and *beta*, and movement velocity in higher frequency rhythm, such as *gamma* (over 32 to 90 Hz) (RICKERT *et al.*, 2005; NAKANISHI *et al.*, 2017). However, it is very complicated to interpret higher frequency characteristics since these are very attenuated in the EEG.

2.3.2 EEG limitation

Given that EEG have an average spatial resolution of up to 10 mm on the scalp (NICOLAS-ALONSO; GOMEZ-GIL, 2012) using the 10/05 electrode placement system, it cannot retrieve enough information about more specific brain regions that are too close to each other. One of the reasons for this difficulty can be seen in Figure 2.7 which shows that there are only a few electrodes directly above the motor control areas and they can still receive much influence from other nearby brain regions.

Therefore, EEG BMIs are best used for classifying between different limb motions instead of retrieving dynamical information from a specific motion (SHAKEEL *et al.*, 2015; Udhaya Kumar; Hannah Inbarani, 2017; LEEB *et al.*, 2015; LOTTE *et al.*, 2007; JERBI *et al.*, 2011).

Fortunately, there are other techniques, such as ECoG and LFP, that can reach a higher spacial resolution and retrieve dynamical information. However, these require surgical procedures, which would cause great discomfort to the subject and are therefore used only in extreme cases such as when the subject already has to undergo such surgery for other medical purposes. Therefore, EEG is still greatly used for many studies involving the analysis of brain activity specially in cases of BMIs.

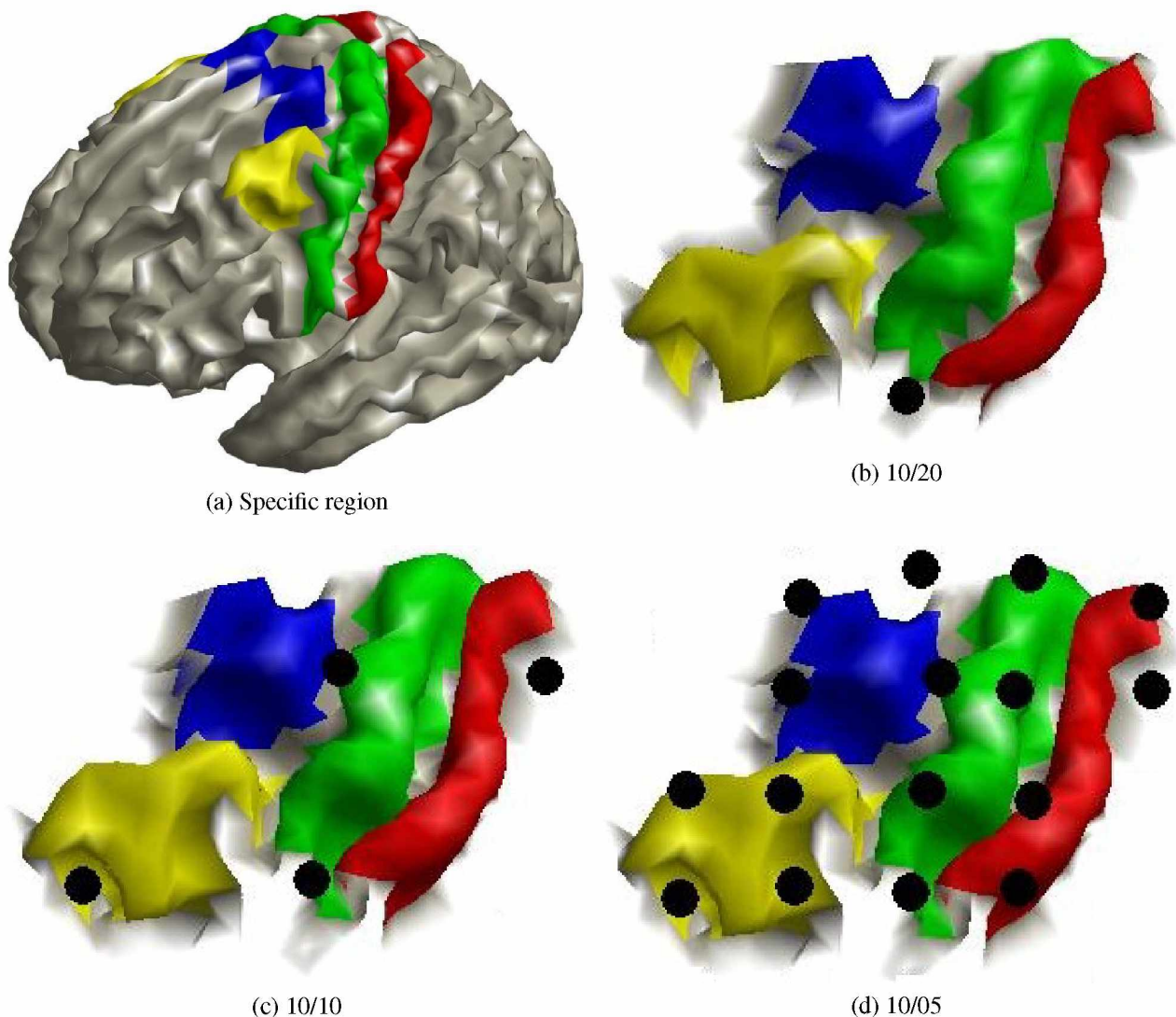


Figure 2.7: (a) Brain regions mostly related to movements: ventral premotor cortex (yellow); dorsal premotor cortex (blue); primary motor cortex (green); and primary somatosensory cortex (red).; (b, c and d) projection of EEG electrodes directly over the specified regions considering different electrode distributions (10/20, 10/10 and 10/05 respectively).

3 ELECTROMAGNETIC SOURCE IMAGING

ESI consists of calculating the internal brain CSs related to each electrical field that influences the EEG recordings (HÄMÄLÄINEN *et al.*, 1993), using prior anatomical knowledge taken from a head model, the EEG signals and a mathematical method. Therefore, ESI can estimate the current values of tens of thousands of CSs inside the brain (JATOI *et al.*, 2014). This translates to a huge spatial resolution increase, not to mention that the CSs have both amplitude and direction, which grants even more information.

These calculated CSs are generated by the dipoles in the brain, previously mentioned, and are the sources for the EEG signals, shown in Figure 3.1. This means that it is possible to acquire information from more specific internal brain signals without the need for surgery.

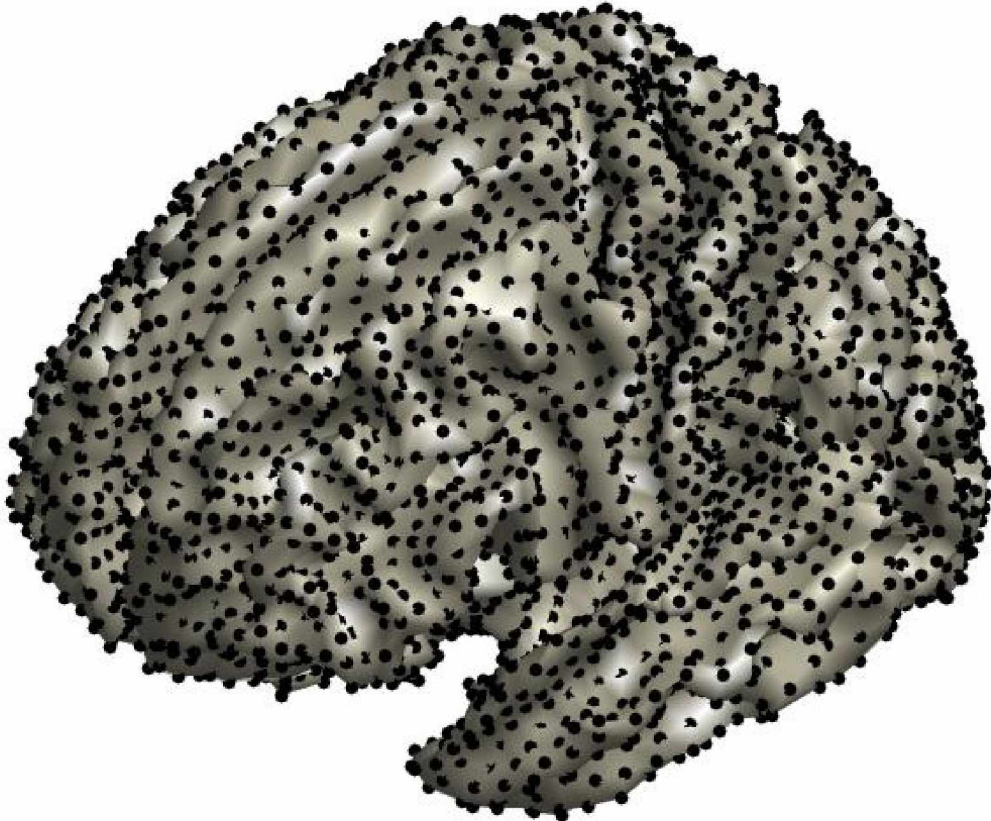


Figure 3.1: CS distribution for a given head model with more than 8000 CSs.

3.1 Applications

ESI has already been applied in several studies, some of them used the CSs signals characteristics to investigate brain connectivity and were able to find satisfactory results (HASSAN *et al.*, 2014; COITO *et al.*, 2016; MAHJOORY *et al.*, 2017). Many others have used ESI to find the epilepsy focal point (BRODBECK *et al.*, 2009; VULLIEMOZ *et al.*, 2010; CUSTO *et al.*, 2014; COITO *et al.*, 2016), which helps to determine with more precision what is the specific region of the brain that should be ablated or stimulated in order to seize the epileptic attacks without jeopardizing the rest of the brain functionality. These epilepsy studies also prove the veracity of ESI calculated signals comparing their results to other methods of finding the epileptic point, and showing their results are precise and in accordance to other methods.

Moreover, recently a few studies have used ESI for analyzing brain motor control. These were able to acquire better results for classification of movements when compared to using standard EEG techniques (HAUFE *et al.*, 2011).

For instance, Edelman, Baxter e He (2016) were able to better classify between different wrist motions (flexion/extension and pronation/supination) when compared to a simple EEG signal classification. Also, Yoshimura *et al.* (2017) investigated single finger motion (only the index finger) in question of position and direction, being able to even point out specific brain regions that were activated during the movement and their probable influences on the motor control.

These studies give further support for investigating the capability of ESI to differentiate between movements from different parts of the same limb.

3.2 Main equation

In order to better understand ESI, it can be summarized in the following equation:

$$C = LS, \quad (3.1)$$

where C is a $N \times t$ matrix with the EEG signals, N is the number of signals, t is the number of samples, S is an $M \times t$ matrix with the CSs signals, M is the number of CSs, and L is the $N \times M$ lead field matrix which determines the influence that each CS has on each electrode.

ESI can be further divided into two main parts: the forward problem, which consists of determining how the CSs will influence the EEG channels through the calculation of the lead field matrix; and the inverse problem, which is the calculation of the CSs using the EEG signals and the knowledge acquired from the forward solution.

3.3 Forward problem

Inside the brain each CS has a dipole moment which generates an electrical field. These electrical fields will propagate through the whole head and reach the EEG electrodes (HÄMÄLÄINEN *et al.*, 1993), therefore, we need to investigate the geometry of the head, the conductivity of its tissues and the locations of the CSs. For this a head model is used.

There are many different methods to construct a head model, and its complexity and resolution will affect the quality of the calculated CSs (FUCHS *et al.*, 2004; HALLEZ *et al.*, 2007; MICHEL *et al.*, 2004). The three most used are: concentric spheres; boundary element method (BEM); and finite element method (FEM) (HALLEZ *et al.*, 2007; JAIR MONTOYA MARTÍNEZ, 2014).

3.3.1 Concentric spheres

The concentric sphere method is the simplest of the methods since it approximates the head to a spherical shape and does the same for all main structures inside it, as presented in Figure 3.2. Usually a concentric sphere model will have one sphere representing the brain, other for the skull and a last one for the scalp (FUCHS *et al.*, 2004).

This approach considers the same conductivity for any space between two spheres, and the CS locations are empirically determined, usually considering an equal spacing near the surface of

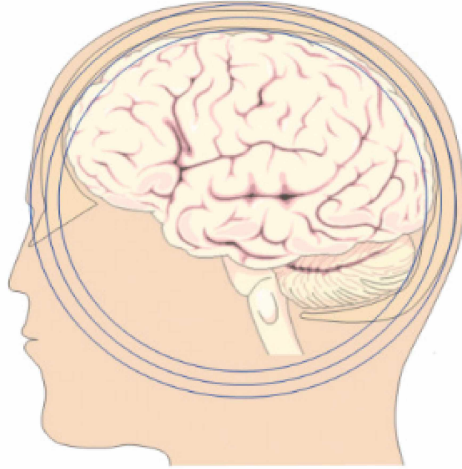


Figure 3.2: Concentric sphere model (adapted from: JAIR MONTOYA MARTÍNEZ (2014)).

the brain sphere. Therefore, although this approach is way simpler than the others it also accounts for greater uncertainties in the CSs's signal reconstruction (HALLEZ *et al.*, 2007).

3.3.2 Boundary element method

BEM grants a better head model, as shown in Figure 3.3, since it calculates the boundaries of the head and its structures using an MRI. That allows for the separation of other structures such as gray and white matter and facilitates to divide each brain region for further analysis. The tissue conductivity is still considered to be equal when inside the same structure, however the CS locations are determined according to the level of precision from the MRI, usually considering only the vertices of the cerebrum surface (HALLEZ *et al.*, 2007).

3.3.3 Finite element method

Though BEM is already a better solution for head modelling the last method, FEM, considers each volume element that can be extracted from the MRI (Figure 3.4) and associates a specific conductivity for each of those. It usually uses images with higher resolutions and therefore demands a way higher level of processing (HALLEZ *et al.*, 2007). So, FEM has the highest precision among these methods, however it also has the highest computational cost.

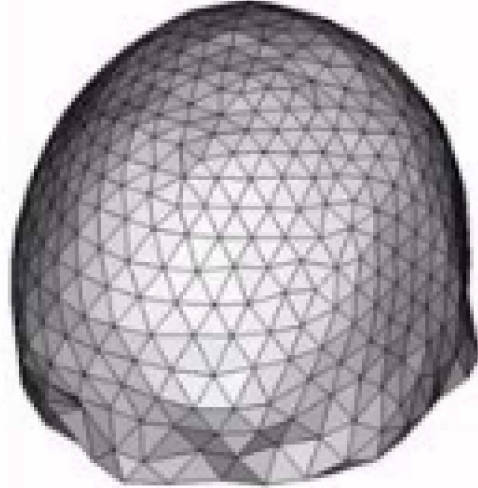


Figure 3.3: BEM model (adapted from: JAIR MONTOYA MARTÍNEZ (2014)).

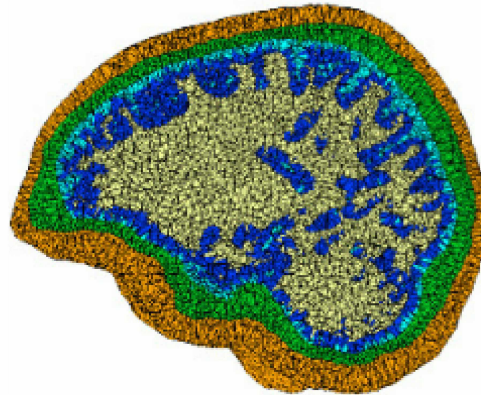


Figure 3.4: FEM model (adapted from: JAIR MONTOYA MARTÍNEZ (2014)).

3.3.4 Lead field matrix

After the head model is constructed, the lead field matrix is calculated considering the tissue conductivity, the position of the EEG electrodes, and the CSs's position and orientation (KOHLER *et al.*, 1996; JATOI *et al.*, 2014).

There are two different approaches to the orientation of the CSs: consider a fixed orientation (usually orthogonal to the surface, considering the pyramidal neurons orientation); or a varying orientation (FUCHS *et al.*, 2004; GRECH *et al.*, 2008; JATOI *et al.*, 2014; MAHJOORY *et al.*, 2017). If a fixed orientation is considered, then the lead field matrix will be an $N \times M$ matrix and S

will be $M \times t$ matrix. However, if the orientation is not fixed then it changes each moment making L an $N \times M \times 3$ matrix and S an $M \times t \times 3$ matrix. Though this last approach might increase the calculations it also allows for more information to be acquired from the ESI application.

3.4 Inverse problem

After determining the lead field matrix we have the values for matrices C and L and can apply an ESI mathematical method to calculate S (solve the inverse problem) in Equation (3.1). However, this problem is ill-posed, having infinite solutions (HÄMÄLÄINEN *et al.*, 1993; JATOI *et al.*, 2014; MAHJOORY *et al.*, 2017).

Therefore, there are several methods that can be applied to solve this problem. The majority of these methods have the same approach using a regularization function $\Omega(S)$ to limit the possible solutions given some prior knowledge about the expected solution. This prior knowledge varies from method to method and can be: limiting the solution to be sparse; making the nearby CSs to have similar signals; and many others (FUCHS *et al.*, 2004; GRECH *et al.*, 2008; JAIR MONTOYA MARTÍNEZ, 2014; JATOI *et al.*, 2014; MAHJOORY *et al.*, 2017).

The use of this regularization function follows the equation:

$$\tilde{S} = \arg \min_S \left\{ \frac{1}{2} \|LS - C\|_F^2 + \lambda \Omega(S) \right\}, \lambda \geq 0, \quad (3.2)$$

where \tilde{S} is the calculated CS matrix, $\|\bullet\|_F^2$ denotes the Frobenius norm, λ is the regularization parameter, an empiric value which limits the influence of the prior knowledge to find the solution.

3.4.1 Minimal norm estimate

Minimal norm estimate (MNE) is an ESI mathematical method which provides a more sparse solution which is better for applications where the signals of dipoles are more likely to extend through an area (HÄMÄLÄINEN; ILMONIEMI, 1994; GRECH *et al.*, 2008).

Its solution can be simplified to the following equation:

$$S = L^+C, \quad (3.3)$$

where L^+ denotes the Moore-Penrose generalized inverse. However this solution is a harmonic function, attaining its maximum values at the boundaries of the domain, which in this case are the most superficial points in the head model. Because of that it is limited in the CS signal reconstruction and localization when compared to new techniques (JATOI *et al.*, 2014).

3.4.2 sLORETA

Standardized low resolution brain electromagnetic tomography (sLORETA) is another ESI method which is widely known and used that in simulations has the lowest localization errors when compared to MNE and can even reach a zero localization error in simulations without noise with a single point source (PASCUAL-MARQUI, 2002; GRECH *et al.*, 2008).

Its regularization function is as follows:

$$\Omega(S) = ||S||^2, \quad (3.4)$$

where $||\bullet||^2$ denotes the 2-norm function. It implies that the internal brain signals have a independent uniformly distributed variance across the brain (JATOI *et al.*, 2014).

3.4.3 eLORETA

Exact low resolution brain electromagnetic tomography (eLORETA) is an ESI method which provides exact localization with zero error in the presence of measurement and structured biological noise (KIMURA; OHIRA; SCHRÖGER, 2010).

The eLORETA method is already well applied and, though it is not the most used one, it grants the advantage of not overestimating superficial sources over deeper ones, as do other greatly used techniques such as minimum norm estimate (JATOI *et al.*, 2014).

For eLORETA the regularization equation is denoted by the following:

$$\Omega(S) = S^T WS, \quad (3.5)$$

where $W \in \mathbb{R}^{(3M) \times (3M)}$ is a symmetric weight matrix calculated from the lead field matrix (L) itself. Yet, λ is still empiric but tied to the noise in the EEG signal, so it can even be assumed as zero in simulation cases, yet for other cases Pascual-Marqui (1999) suggested a method using a cross-validation error.

3.5 Data analysis

3.5.1 Sources of interest

Even limiting the analysis to consider only a specific brain region, there are usually many source points inside these regions requiring the application of a dimensional reduction technique.

Since it is well known that *mu* rhythms are highly related to movement control (NICOLAS-ALONSO; GOMEZ-GIL, 2012; MCFARLAND *et al.*, 2000), many EEG applications use principal component analysis (PCA) over the *mu* power levels to extract only the information most related to the highest variance in signal for this specific rhythm. Though this would be optimal for applications in motor control analysis, since it is required to find the CSs with highest activity change, hence variety, PCA transforms the signal into a different spacial representation so that the resulting signals are no longer related to a specific source point in the brain, but rather a linear composition from each individual source point.

However, we can still use this knowledge for comparing the difference in total *mu* power between different time intervals. The CSs with highest change in *mu* power between an interval before motor planning (theoretically not related to brain activity) and an interval during motor planning (before movement onset (start)) will most likely be more relevant for motor planning. Likewise, the CSs with highest change in *mu* power between an interval during motor planning and an interval during motor execution will most likely be more relevant for motor execution.

3.5.2 Recalculated average direction

In the case of calculating the CSs without a fixated orientation, the complexity of signal analysis becomes way higher, because now there are three values for each sample of each CS. We can use the power levels for simpler analysis (such as dimension reduction), but when it comes to time and frequency visual analysis it would be important not to lose this orientation information.

Fortunately, Coito *et al.* (2016) applied a technique named recalculated average direction (RAD) which consists of determining the resulting direction of each CS for a given time interval considering only the 90% strongest directions. Then each sample inside this time interval is recalculated as a projection over the resulting direction of each CS.

4 METHODOLOGY

For proving our hypothesis we proposed to find the most relevant source points during different movement activities in the same limb applying ESI to EEG signals and then analyse the time and frequency changes within the signals from those sources to verify if they are in accordance to prior knowledge about the brain motor control.

We divided the whole process into two main stages: validation; and application. The methods and materials needed for these processes are further explained in this chapter.

4.1 Lead field calculation

The lead field matrix changes according to the head model, the tissue conductivity, the number of internal source points, and the number of EEG electrodes. However, since we used a previously collected data set, we did not have access to MRI data from each of the subjects. Therefore, we turned to an MRI data set which is commonly used in ESI applications (MAHJOORY *et al.*, 2017), the icbm152 data set. It consists of an averaged head MRI from 152 different subjects (MAZZIOTTA *et al.*, 1995; FONOV *et al.*, 2011), allowing for general applications in cases where there are no available specific MRI data. Even though there might be some inaccuracies inherited from such approximation, this data set provides an approximation which is sufficient for more general application such as the one in this study.

Having determined the head model from the icbm152 data set (MAZZIOTTA *et al.*, 1995), the vertices from the calculated brain surface model were considered as source points, resulting in 8196 source points throughout the brain (with an average distance between each other of 3.67 mm), as illustrated in Figure 4.1. The electrode positions were considered according to the 10/10 system having 64 electrodes, also illustrated in Figure 4.1. Later we recalculated the lead field matrix for the same CSs but with a different arrangement of electrodes to fit correctly the used EEG data set.

Furthermore, the tissue conductivities were considered as 0.3300 Sm^{-1} , 0.0042 Sm^{-1} , and 0.3300 Sm^{-1} for brain, skull and scalp respectively (WANG; REN, 2013).

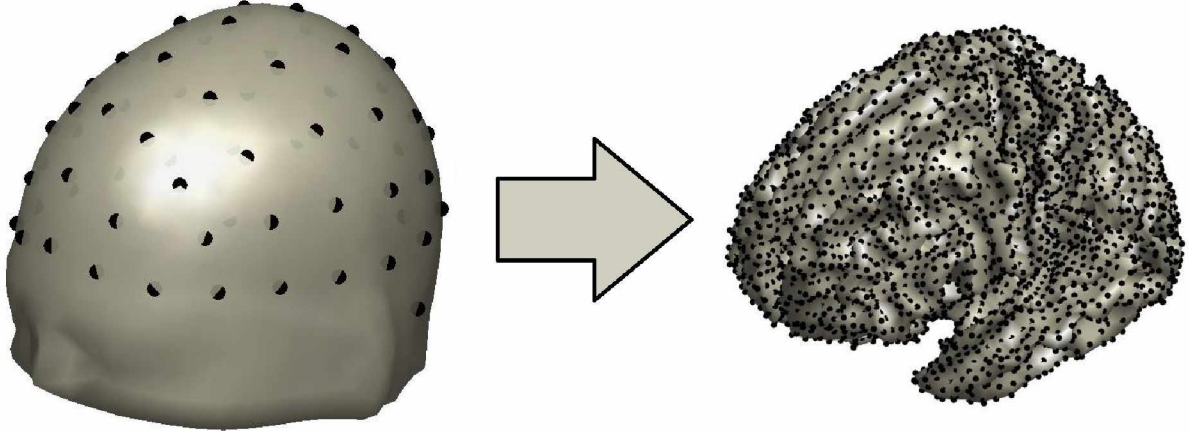


Figure 4.1: Used electrode and source positions.

All calculations were made with the MATLAB[®] functions from the FieldTrip[®] toolbox (OOSTENVELD *et al.*, 2011).

4.2 Validation with simulated signals

Although eLORETA is well known, it is important to prove its validation. And since we did not have access to any ways for recording internal brain signals in order to have the exact values for the S matrix, this validation is done using simulated signals, as it is usually done for many ESI methods (KIMURA; OHIRA; SCHRÖGER, 2010; GRAMFORT *et al.*, 2013; COSTA *et al.*, 2017).

Using a simulated data generated for matrix S , and the lead field matrix, the C matrix is calculated using Equation (3.1). These values are then used to calculate \tilde{S} using Equation (3.2). After that, the method is validated through the comparison between the values in matrices S and \tilde{S} .

We simulated CS signals in different settings, generated electrode signals in a 10/10 system using Equation (3.1). After that we applied eLORETA, using $\lambda = 0$, since it is a simulation, and compared the calculated CSs to the original ones using several different metrics.

In order to further solidify the better performance from eLORETA, we also applied other two methods to the simulation settings: Minimum norm estimate (MNE) (HÄMÄLÄINEN *et al.*, 1993; HÄMÄLÄINEN; ILMONIEMI, 1994); and standardized low resolution brain electromagnetic tomography (sLORETA) (PASCUAL-MARQUI, 2002).

4.2.1 Signal generation

We generated four different simulated signals using the icbm152 head model. These simulations differed in number and position of activated CSs which are presented in Table 4.1 and Figure 4.2.

Table 4.1: Number of sources and their general positions for each CS simulation.

# activated sources	Positions
1	left M1
1	right M1
3	2 left M1; 1 right M1
10	5 left M1; 2 left S1; 3 left occipital cortex

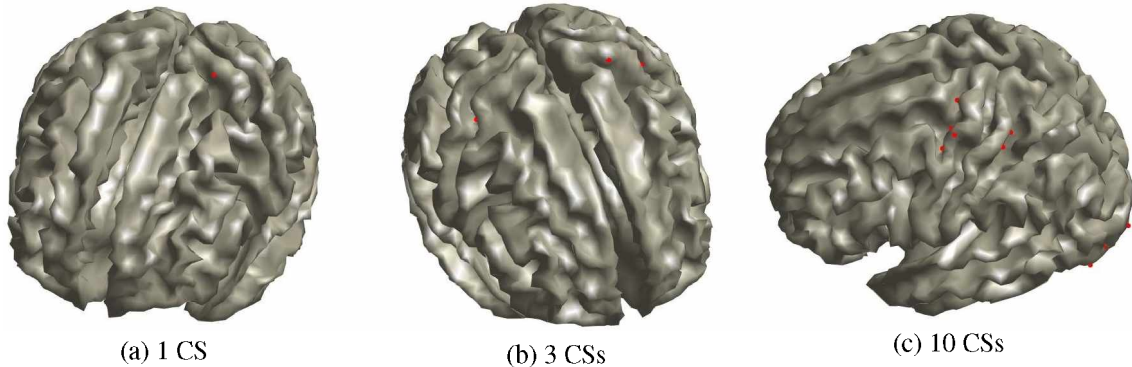


Figure 4.2: (a, b and c) CSs chosen for the simulations with 1, 3 and 10 main CSs respectively.

The generated signals were comprised of Morlet Wavelets with a central frequency of 12 ± 4 Hz and a decay frequency of 0.175 ± 0.125 Hz. The signals had a duration of 1.2 s and a sampling frequency of 512 Hz, however the wavelets only have a duration of 0.60 s and had varying temporal displacements as illustrated in Figure 4.3. Since each CS has signal components to each dimension, we generated three different simulated signals to each activated source, also shown in Figure 4.3.

We also added a background activity by adding a white noise to all CSs (even the ones that were not used) with a signal to noise ratio (SNR) of 20 dB, and filtering all of them with a low-pass filter of 40 Hz and a high-pass filter of 1 Hz. That way, the background would have a frequency within the strongest brain rhythms (NICOLAS-ALONSO; GOMEZ-GIL, 2012).

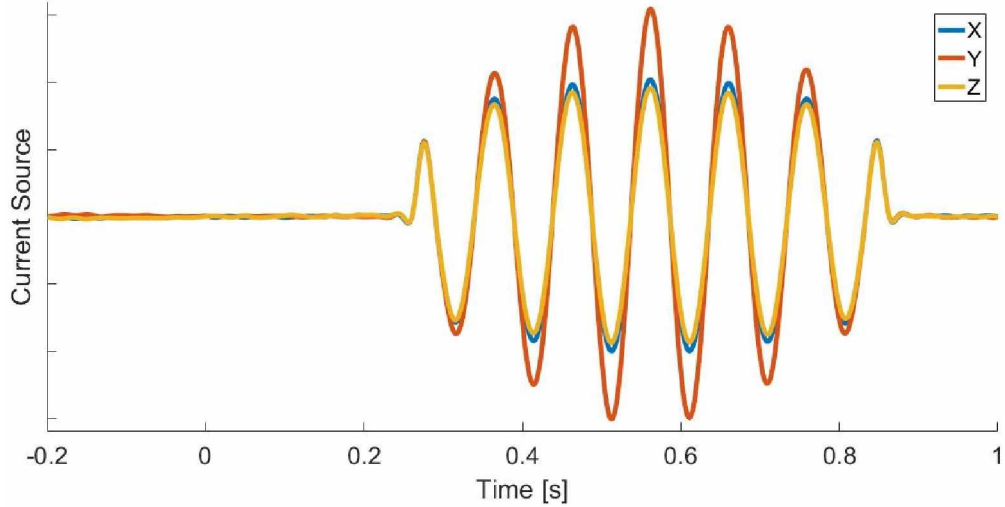


Figure 4.3: Example of simulated signals for each direction of one CS.

4.2.2 Comparison metrics

The comparison metrics that we used were chosen to better analyse not only if the signals were correctly reconstructed but also if the positions were correct. Keeping in mind that there could be a situation where the signal is correctly reconstructed but with slight position differences.

4.2.2.1 Correlation coefficient

The correlation coefficient (CC) between two sets of data represents the probability of a mathematical/statistical relationship between the two (MUKAKA, 2012), as presented in the following equation:

$$r = \frac{\sum_{i=1}^n (x_i - \bar{x})(y_i - \bar{y})}{\sqrt{(\sum_{i=1}^n (x_i - \bar{x})^2)(\sum_{i=1}^n (y_i - \bar{y})^2)}}. \quad (4.1)$$

Therefore, the higher the coefficient, the stronger the relationship between the data sets. If the data sets are equal, then it retrieves a maximum value of 1, and if they are exactly opposite then the value will be -1.

In the case of CSs, it can be used in two different ways:

- In the 1 to 1 comparison (Total CC) each source from the S matrix is compared to its counterpart in the \tilde{S} matrix, analysing the reconstruction accuracy for each source position;

- In the 1 to all comparison (Focal CC) only the main sources from the simulated data (S) are considered, and for each of them the correlation coefficients are calculated in relation to every CS in the calculated matrix (\tilde{S}), analysing if the main source signals were correctly calculated. This can also be applied to the main sources from the simulated data in comparison to the found main sources in the calculated data. Therefore there is a true Focal CC and a found Focal CC.

4.2.2.2 Distance between main sources

Using the Total CC the found CSs with highest correlation to the original ones might be in a different position. It is important to calculate this distance, for it shows what is the average spread of signal that the method generates.

4.2.3 Further validation

Since we encountered some problems to more accurately simulate internal brain signals, we needed a better way to validate eLORETA.

Therefore, we used one of the real EEG data segments and considered it as a simulated source (S). Then we calculated the EEG signals (C) using Equation (3.1) and found \tilde{S} by applying eLORETA to it. We then compared these matrices using the same metrics applied in the previous simulations.

4.3 Application with real data

After validating the method, we applied it to a data set with EEG signals sampled during the performance of different movements from the same limb, in order to analyse if the behaviour of calculated internal signals during these movements is in accordance to prior literature knowledge.

4.3.1 Data set

The data set was acquired from Ofner *et al.* (2017). It had EEG signals from 15 different healthy subjects between 22 and 40 years with a mean age of 27 years. Nine subjects were female, and all the subjects except s1 were right-handed. These subjects performed with their right upper limb the following movements: hand closing and opening; wrist pronation and supination; and elbow flexion and extension. The EEG had 61 channels selected from the 10/05 system (with an average distance of 24.69 mm between each other), mostly concentrated in the central region of the brain as presented in Figure 4.4, and had a sampling frequency of 512 Hz. The data set also included electrooculogram (EOG) signals which were used to filter any artifact related to eye movement in the EEG signals.

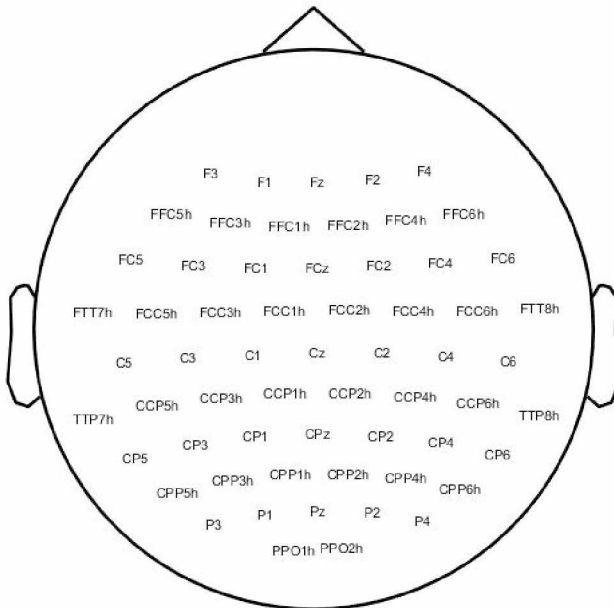


Figure 4.4: EEG channels used for data collection.

Each subject had their arms supported by an exoskeleton with anti-gravity support to avoid muscle fatigue and had a screen in front of them which would indicate which movement to perform. The signals from the exoskeleton and from a data glove were also sampled in order to determine the several movement onsets. All movements had a maximum, a rest and a minimum point, therefore, they were normalized so that the rest point would value 0 and the maximum and minimum would have values of 1 and -1 respectively.

In total, each subject performed 10 sampling runs, where each run had 6 instances from each movement class, making a total of 60 movements for each class. Further explanation from the data set can be found in the original paper: Ofner *et al.* (2017).

4.3.2 EEG preprocessing

The EEG signals were filtered with low pass and high pass filters with cut-off frequencies of 1 and 90Hz respectively, and further filtered with notch filters for 50 and 100 Hz to eliminate the power line interference.

The eye movement influence was minimized using Independent Component Analysis (ICA), having the three EOG channels as basis to find the components most related to the eye movement. This step was done through visual and automatic analysis, where the independent components with highest correlation to the EOG signals were eliminated along with other ones which were considered as noisy in the visual analysis as exemplified in Figure 4.5.

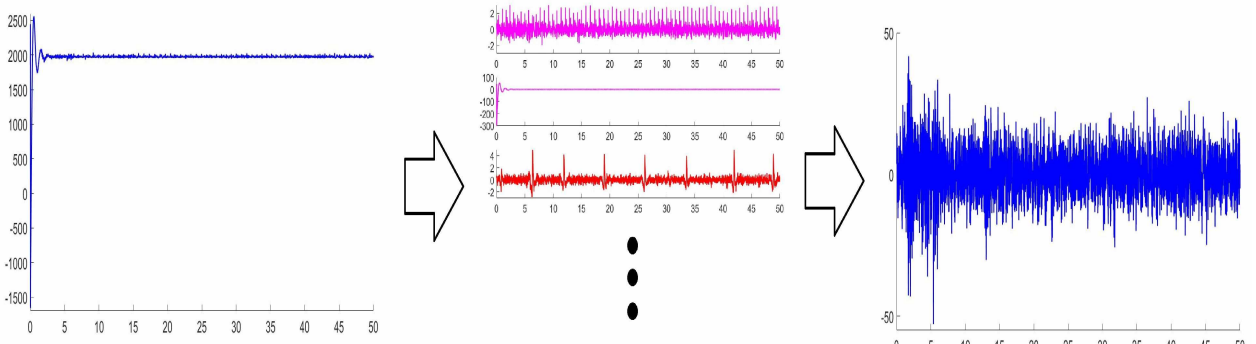


Figure 4.5: EEG ICA decomposition and eliminated components through correlation with EOG (red) and visual analysis (magenta).

EEG signals were then windowed using the onsets of movement acquired from the data glove and exoskeleton signals. The window comprised of 1 s before the beginning of movement and 3 s after it, as shown in Figure 4.6.

The onsets for each movement were determined from exoskeleton and data glove channels which were chosen given ease of finding these sampling moments for every instance of movement. These were: exoskeleton ‘Elbow’ channel for both elbow movements; exoskeleton ‘ProSupination’

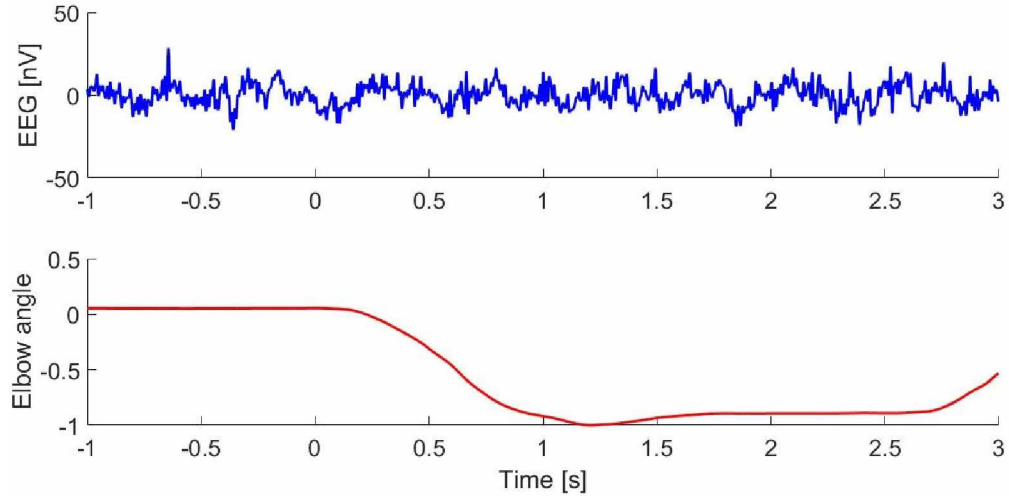


Figure 4.6: Example of window from EEG channel C3 and the exoskeleton elbow signal (normalized) used to determine the movement onset.

channel for both wrist movements; exoskeleton ‘GripPressure’ channel for hand closing; and data glove ‘ring_near’ channel for hand opening.

4.3.3 ESI calculation

After windowing the EEG signals, they were all used in ESI calculations using eLORETA to determine the CS signals for each movement occurrence separately, then we delimited region of interest (ROI), used a dimension reduction to minimize the number of CSs, calculated the RAD values for the CSs inside of it, and finally analysed their signals.

4.3.3.1 Regularization parameter

First, we needed to determine the regularization parameter (λ). For eLORETA, this can have values above or equal to zero. To determine this value, we applied a genetic algorithm, which is an evolutionary algorithm that searches the optimal solution for a determined problem (fitness function) by manipulating a population of possible solutions (individuals). The individuals are evaluated given their results in the fitness function, then a new generation of individuals is selected from the previous given some manipulations such as crossing over the previous individuals and even mutating them (these techniques vary from application to application) and then the process

repeats for the new generation of individuals. Finally the algorithm stops after reaching a certain condition such as number of generations or a threshold in the fitness function.

Since it is possible to determine the EEG signals from the CS signals using Equation (3.1), we used the minimum squared error between the original EEG signals and the signals calculated from the estimated CSs as fitness function, and our individuals were possible values for λ .

The other genetic algorithm parameters were chosen somewhat empirically and are further listed: uniform creation function; scattered crossover function; 0.8 crossover rate; elitism count of 2; a function tolerance of 10^{-10} ; 100 maximum generations; 10 maximum stall generations; Gaussian mutation function; population size of 50 individuals; roulette selection function; and value limits for the population between 25 and 10^{-11} .

4.3.4 Region of interest

The information went from a 61 EEG channel space to a 8196 CS point space, requiring a dimension reduction for simplifying the analysis.

We separated only the CS points within the brain areas most related to the performed movements as our ROI. These areas were selected only from the left hemisphere, since all movements were performed with the right-arm and are presented in Figure 4.7. They were: vPM; dPM; upper half from the M1; and upper half from the S1.

It is important to mention that even with the separation of this ROI, the spatial resolution increase is still huge: from about 8 electrodes over the ROI to 491 CSs inside it, as illustrated in Figure 4.8.

4.3.5 Dimension reduction

Even after separating the ROI, we had 491 CSs to work with, so we had to apply a dimensional reduction to limit the number of CSs we would work with.

We compared the changes in power levels in the *mu* rhythm for each CS and found the ones mostly related to movement planning and the ones mostly related to movement execution. From these we chose only the strongest SC from each sub-region inside our ROI (vPM, dPM, M1 and

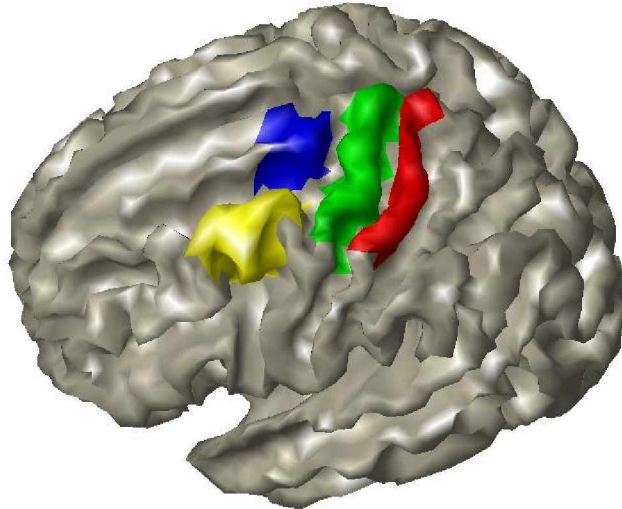


Figure 4.7: Brain ROIs separated for dimension reduction: vPM (yellow); dPM (blue); upper half from the M1 (green); and upper half from the S1 (red).

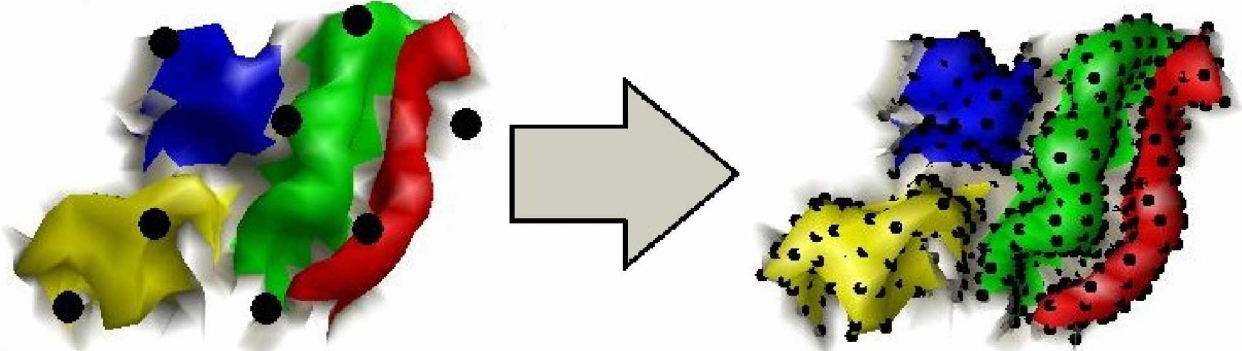


Figure 4.8: Electrodes used in the data set acquisition and CSs found right above and inside the ROI (respectively).

S1), however, M1 had two CSs to account for the fact that hand and elbow movements are mostly related to two different regions within M1.

4.3.6 ESI analysis

After determining the most relevant CSs for each movement, their RAD signals were calculated and analysed, along with the power levels for the motion from all limb sub-parts (hand, wrist and elbow), with a geographical position analysis (firstly considering all CSs in the ROI).

However, it would be better to see differences along the time, and this is more complicated to show in paper using the previous method. Therefore, we calculated the spectrogram from the

RAD values of the most relevant CSs. For that we used a Hamming window of 0.25 s and a step of 1 sampling point (0.002 s). We are then able to analyse time-frequency changes in the signal up from 4 Hz, given the chosen window size.

In order to further analyse the differences between limb sub-parts, we made a separate single window with approximately 21.5 second which contained one movement from each limb sub-part. We then applied ESI to it, followed by the RAD calculation, considering the relevant CSs previously found. Then the time and frequency analysis were performed in the same way as mentioned above.

5 RESULTS AND DISCUSSIONS

5.1 Stage 1: Validation using simulated data

We used simulated sources and calculated the EEG signals from them to investigate how well ESI could reconstruct the CSs. Figures 5.1 to 5.3 show the power levels of CSs for both simulated and calculated sources considering 1 and 10 activated sources. Giving a general evaluation of how similar ESI can reconstruct the CSs.

With Figures 5.1 to 5.3 we can estimate that there was a spread of the signal from the main CSs throughout the brain. Therefore, in order to analyze quantitatively the reconstruction, we calculated the Total CC, considering every CS, and the true and found Focal CC, considering only the CSs with highest significance, and the average distance between the simulated and calculated activated sources. Table 5.1 present these results considering the different number of activated sources. With these values we can determine how well the ESI can reconstruct the CSs (Total CC) and weather the main differences are in source location (specific point distance) or source waveform (Focal CC).

Table 5.1: Total CC, Focal CC, and specific point distance between simulated and calculated sources in all cases (1, 3 and 10 focal points) for the eLORETA method.

# activated sources	Total CC	Focal CC (true)	Focal CC (found)	Distances [mm]
1 (left)	0.1223	0.9949	0.9949	0.0000
1 (right)	0.1800	0.9718	0.9718	0.0000
3	-0.1140	0.9198	0.9768	14.7201
10	-0.1378	0.7062	0.8311	52.5590

The results in Table 5.1 prove that eLORETA provides exact localization with zero error when considering a point source (KIMURA; OHIRA; SCHRÖGER, 2010), however, this was only analysed in the cases with only one main CS. The cases with 3 and 10 main CSs showed a non-negligible localization error. However, both calculations of Focal CC, for true and found main CSs, were higher than 0.9 even for the case with 3 main CSs, but went down to approximately 0.7 in the

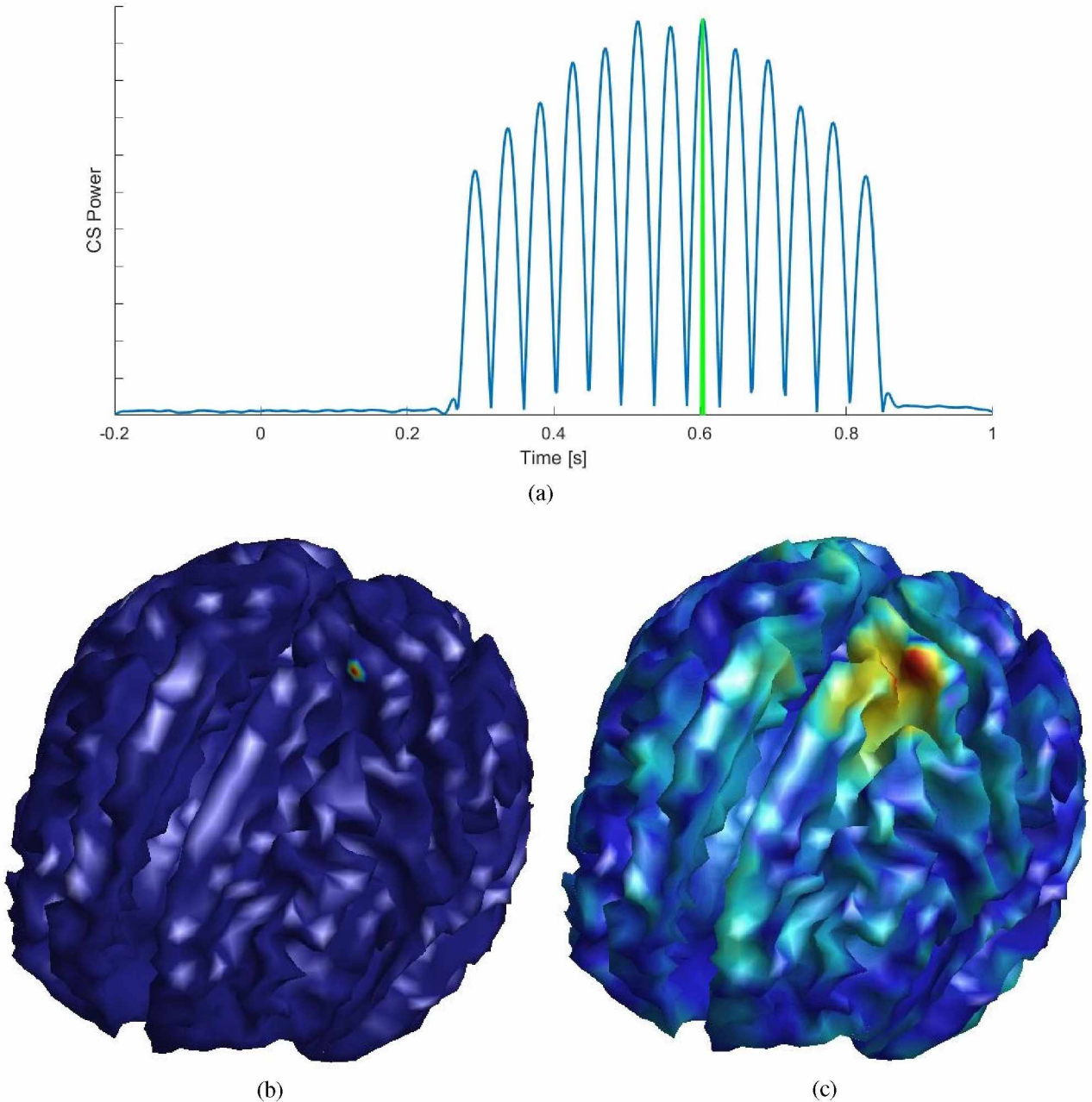


Figure 5.1: Simulation using 1 main CS. (a) power from the main CS and a cursor indicating the time sample for the following subfigures; (b and c) CS power in a specific time sample from the simulated and calculated source spaces respectively.

case with more than 10 mains CSs. However, the Total CCs, were kept around 0.1 and 0.2 for all simulations, inferring a bad reconstruction of the overall sources.

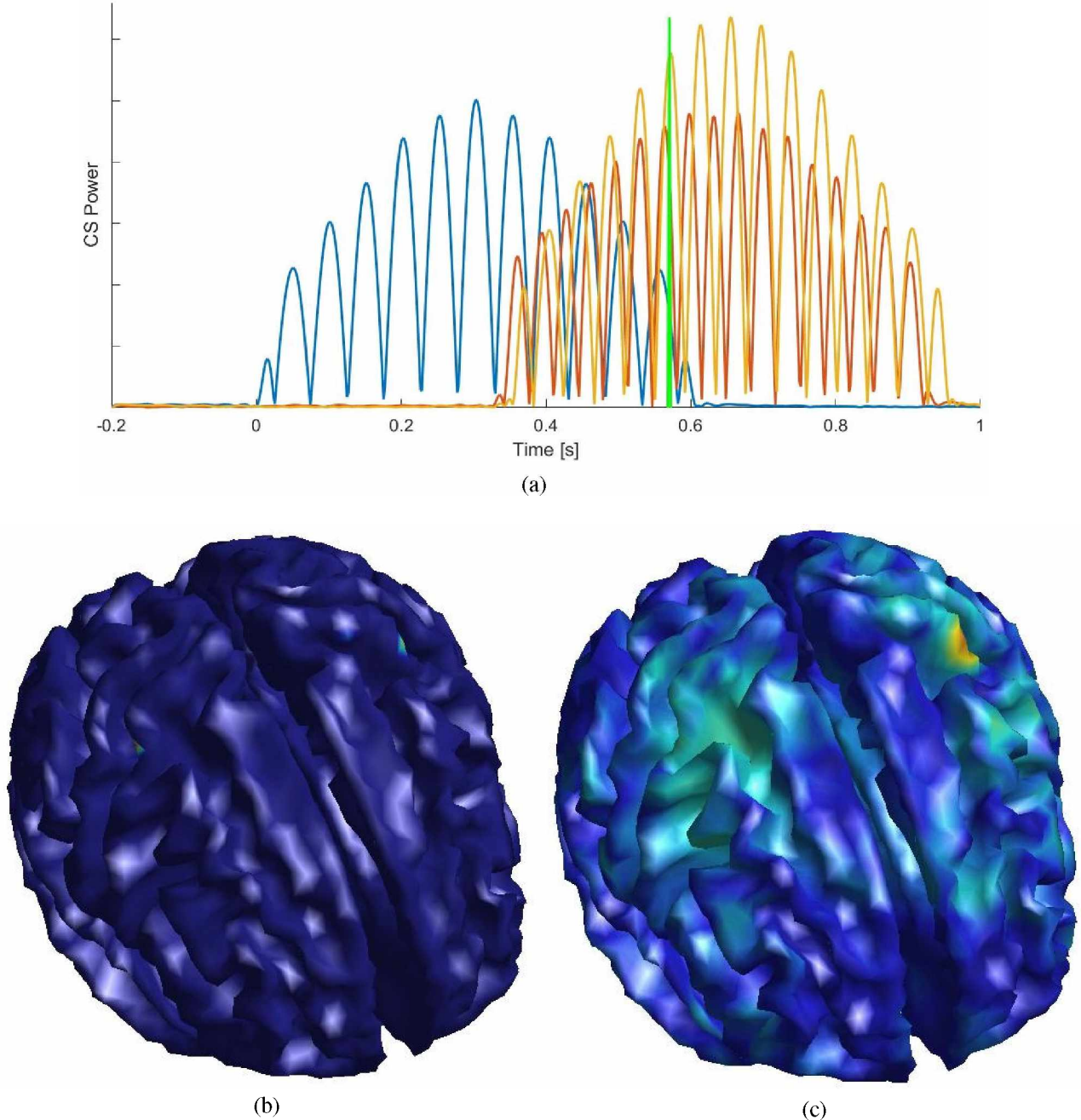


Figure 5.2: Simulation using 3 main CSs. (a) power from the main CSs and a cursor indicating the time sample for the following subfigures; (b and c) CS power in a specific time sample from the simulated and calculated source spaces respectively.

We can also compare the results regarding the other methods (MNE and sLORETA), shown in Tables 5.2 and 5.3. We see that the results are very similar for Total em Focal CC, however the values from eLORETA are higher on average. But there is a great difference regarding the distance

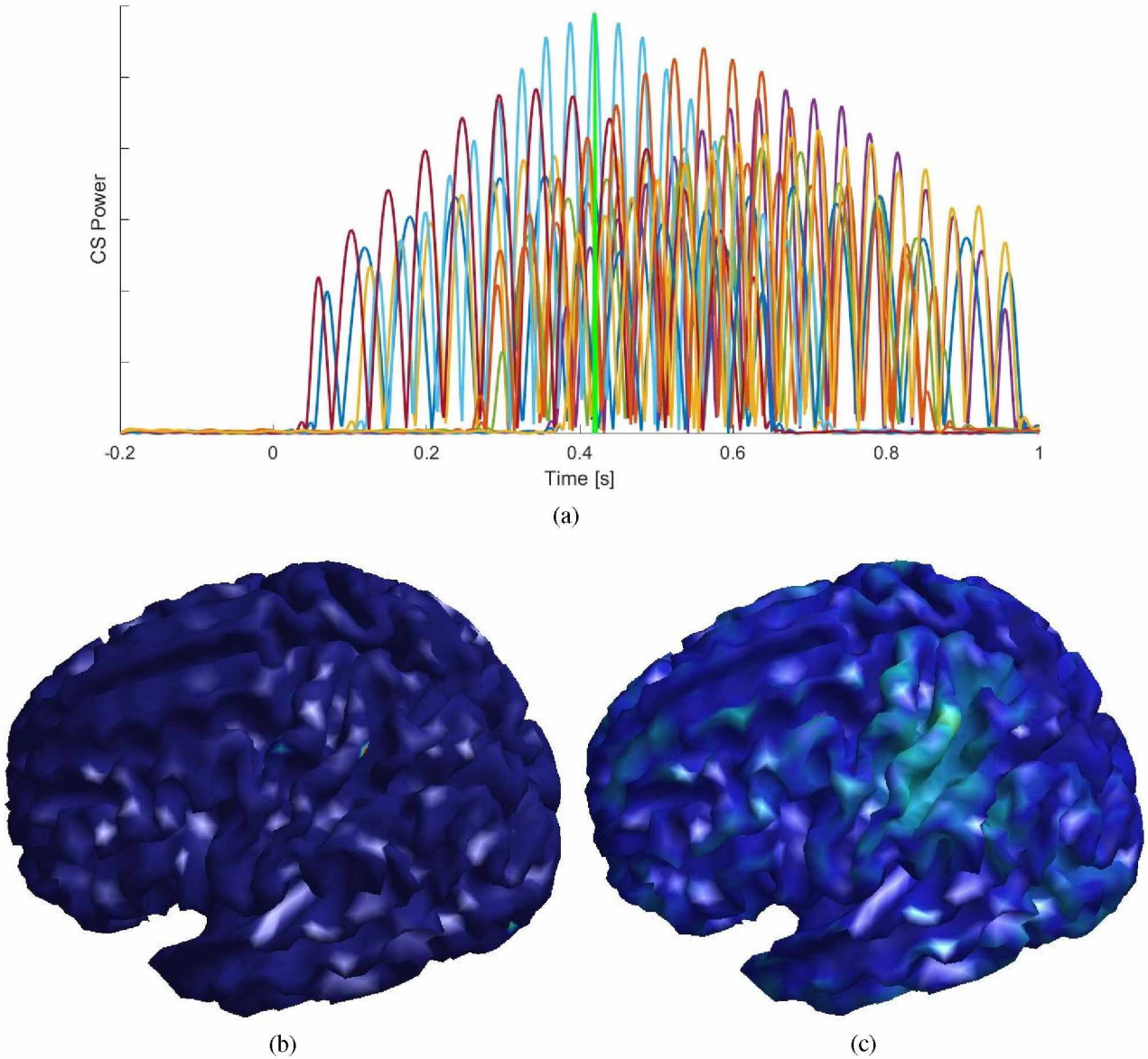


Figure 5.3: Simulation using 10 main CSs. (a) power from the main CS and a cursor indicating the time sample for the following subfigures; (b and c) CS power in a specific time sample from the simulated and calculated source spaces respectively.

error, where the distances from true to found main CSs were smaller for the eLORETA results. Therefore, we chose to apply eLORETA for the rest of the study.

Furthermore, we decided to rerun the simulations with 10 activated sources, yet this time we left the source position to be random and repeated the process 100 times to avoid any biases. The result is presented in 5.4.

Table 5.2: Total CC, Focal CC, and specific point distance between simulated and calculated sources in all cases (1, 3 and 10 focal points) for the sLORETA method.

# activated sources	Total CC	Focal CC (true)	Focal CC (found)	Distances [mm]
1 (left)	0.0819	0.9972	0.9972	0.0000
1 (right)	0.1102	0.9805	0.9916	18.6095
3	-0.1287	0.9603	0.9844	9.8241
10	-0.1119	0.7020	0.8417	85.9916

Table 5.3: Total CC, Focal CC, and specific point distance between simulated and calculated sources in all cases (1, 3 and 10 focal points) for the MNE method.

# activated sources	Total CC	Focal CC (true)	Focal CC (found)	Distances [mm]
1 (left)	0.0512	0.9586	0.9648	4.5560
1 (right)	0.1220	0.9526	0.9582	8.5149
3	-0.1168	0.9417	0.9565	16.9831
10	-0.0974	0.6542	0.8110	86.0341

Table 5.4: Averages of Total CC, Focal CC, and specific point distance between simulated and calculated sources having 10 random sources activated for the MNE, sLORETA and eLORETA methods.

Method	Total CC	Focal CC (true)	Focal CC (found)	Distances [mm]
MNE	-0.0959	0.6192	0.7849	42.9935
sLORETA	-0.0965	0.6698	0.8081	39.9807
eLORETA	-0.0705	0.6703	0.7973	35.1194

However, there were still some inaccuracies. Though these are in accordance to Figures 5.1 to 5.3, they might be due to a lack of biomimetism in them. For instance, a noise signal between 1 to 40 Hz was added to serve as background brain activity, however, this noise signal was added with an SNR of 20 dB, which might not be an accurate value. And we did not change the signals of surrounding CSs to be somewhat similar to the main ones as it is estimated by the eLORETA method itself.

Because of these results and limitations in our simulations, we applied a similar analysis in real EEG data. We used a calculated source signal from a real EEG data as original CS signal, from it we calculated the EEG signal and then recalculated the CS signals. We then compared them using the same measurements. The results were way better, as presented in Table 5.5 and Figure 5.4 showing a way similar reconstruction. This shows that the simulation was not optimal for proving

the accuracy of total CS reconstruction, but rather focal CS reconstruction. However, the method can still be used for broader brain activation considering the results from the real EEG signals.

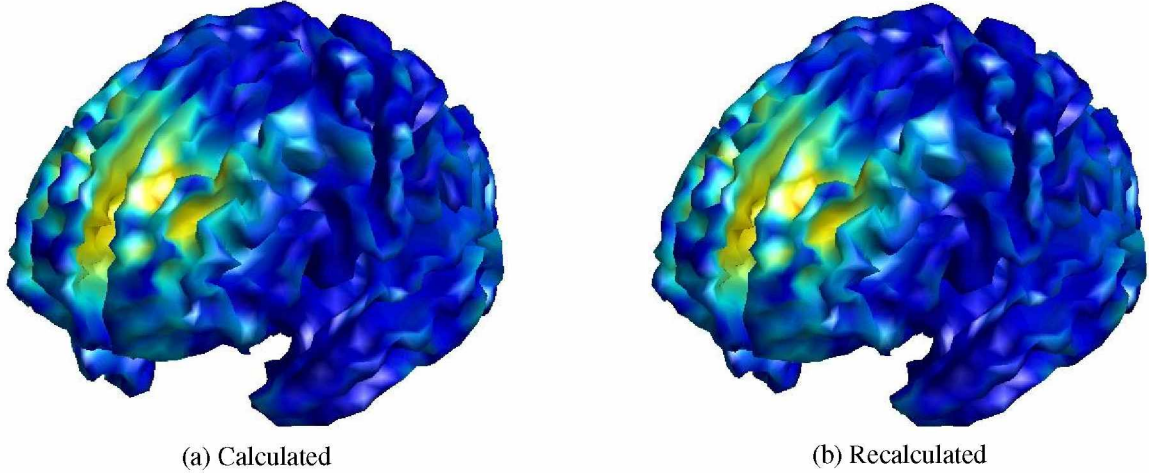


Figure 5.4: Source space calculation and recalculation using real EEG data. (a) shows the CSs calculated from a real EEG signal. (b) shows the CSs recalculated from an EEG which was calculated from (a).

Table 5.5: Total CC, Focal CC, and specific point distance between simulated and calculated sources in real data for the eLORETA method.

Total CC	Focal CC (true)	Focal CC (found)	Distances [mm]
0.8144	0.9900	0.9935	15.5735

5.2 Stage 2: Application using real EEG signals

Knowing how reliable ESI's reconstruction is, we investigated if the reconstruction from real data grants enough information and if it corresponds to prior literature knowledge.

For that we used an EEG data set with data from 15 individuals performing different right arm movements and applied ESI to it.

5.2.1 Regularization parameter

We applied a genetic algorithm for finding the best value for the regularization parameter λ by minimizing the error between the original EEG signal and the one calculated by applying Equa-

tion (3.1) to the calculated CSs. The results from the genetic algorithm reached a minimum error of 3.4022×10^{-12} with $\lambda = 1.0000 \times 10^{-11}$ which was the minimal value which the genes could reach. Figure 5.5 shows the huge tendency for lower errors considering smaller λ values.

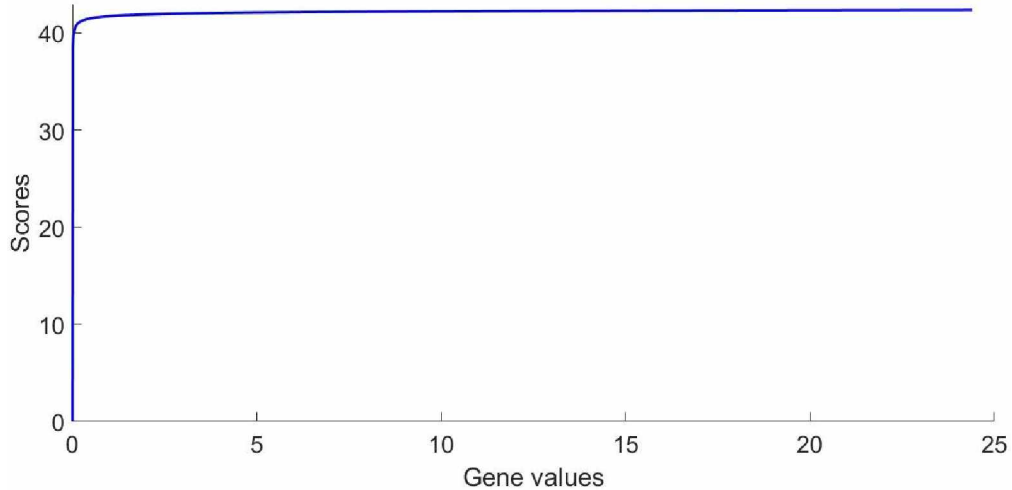


Figure 5.5: Convergence from the genetic algorithm for finding the best gene (λ) value by finding the minimal score (error) value.

Since the found value for λ was so close to zero, we also made a test with $\lambda = 0$ assuming that the genetic algorithm did not reach this value due to the empirical values chosen. This λ value reached an error of 3.0827×10^{-18} , which is even lower than that from the value found using the genetic algorithm. Hence, all ESI calculations here onward use $\lambda = 0$.

5.2.2 CS power and RAD analysis

After reconstructing the CSs, we analysed the RAD and power levels temporally by comparing the activities regarding different moments during the whole movement planning and execution. Figures 5.6 to 5.11 show these values for the onset moment for three different occurrences from each movement class. However, the supplementary material contains animated Figures for each of these occurrences in the material present in the following database: <<https://1drv.ms/u/s!AgVspuYPRFipjsskmJapXK2QSmxkjQ?e=vse1xj>>.

Through these images we are able to see that indeed RAD grants more information from the CSs in comparison to the power levels. However, we are going to focus on the power levels for

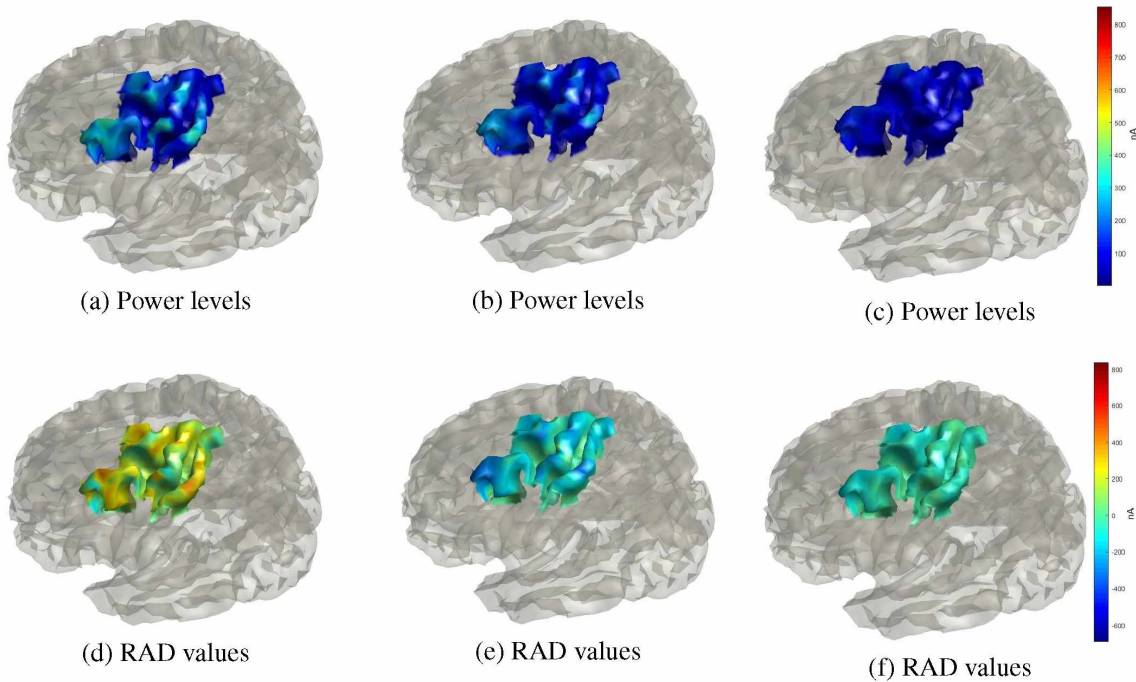


Figure 5.6: CS's RAD and power levels from the onset instant for different hand opening movements for a single subject. (a,b,c) Power levels; (d,e,f) RAD values.

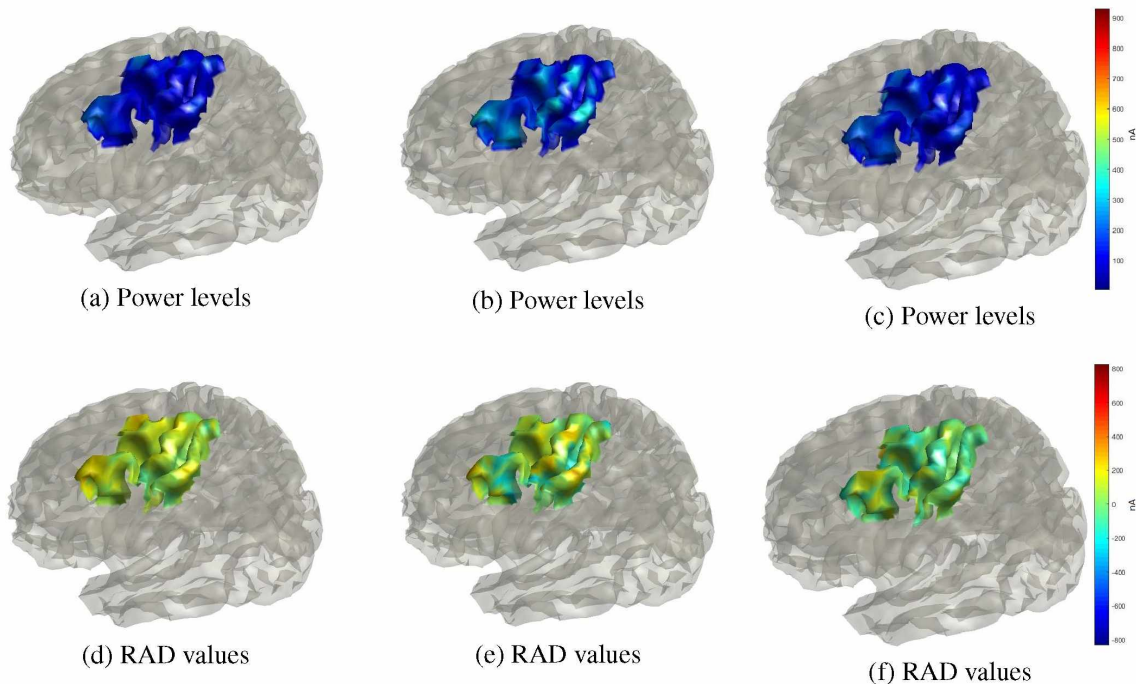


Figure 5.7: CS's RAD and power levels from the onset instant for different hand closing movements for a single subject. (a,b,c) Power levels; (d,e,f) RAD values.

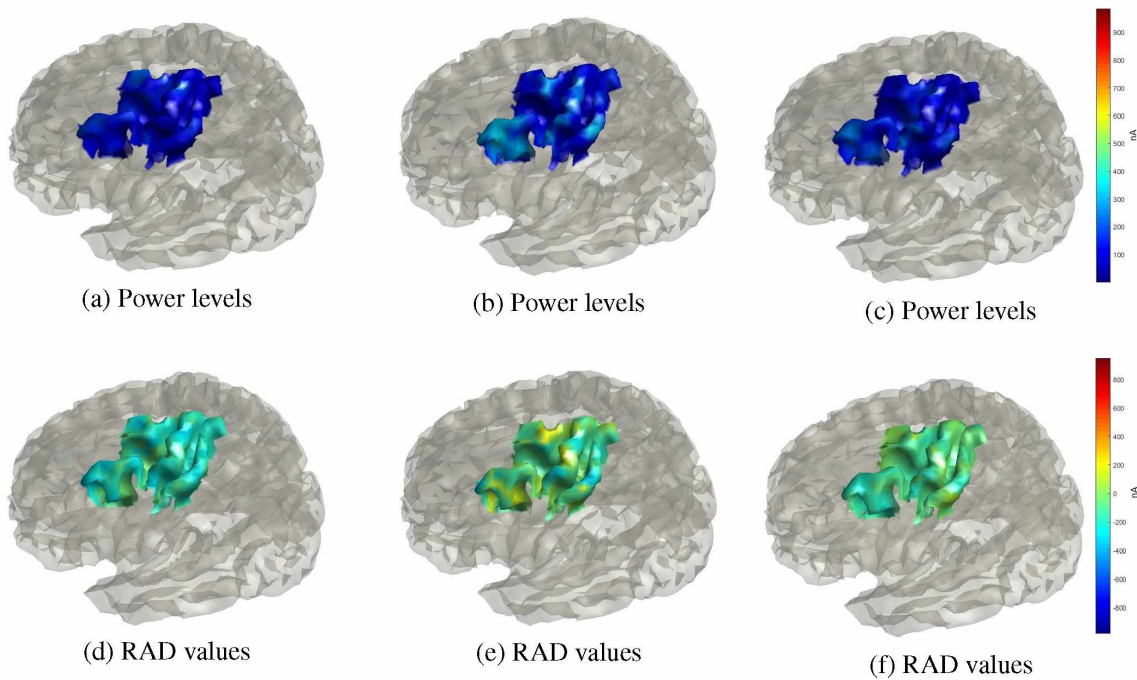


Figure 5.8: CS's RAD and power levels from the onset instant for different wrist supination movements for a single subject. (a,b,c) Power levels; (d,e,f) RAD values.

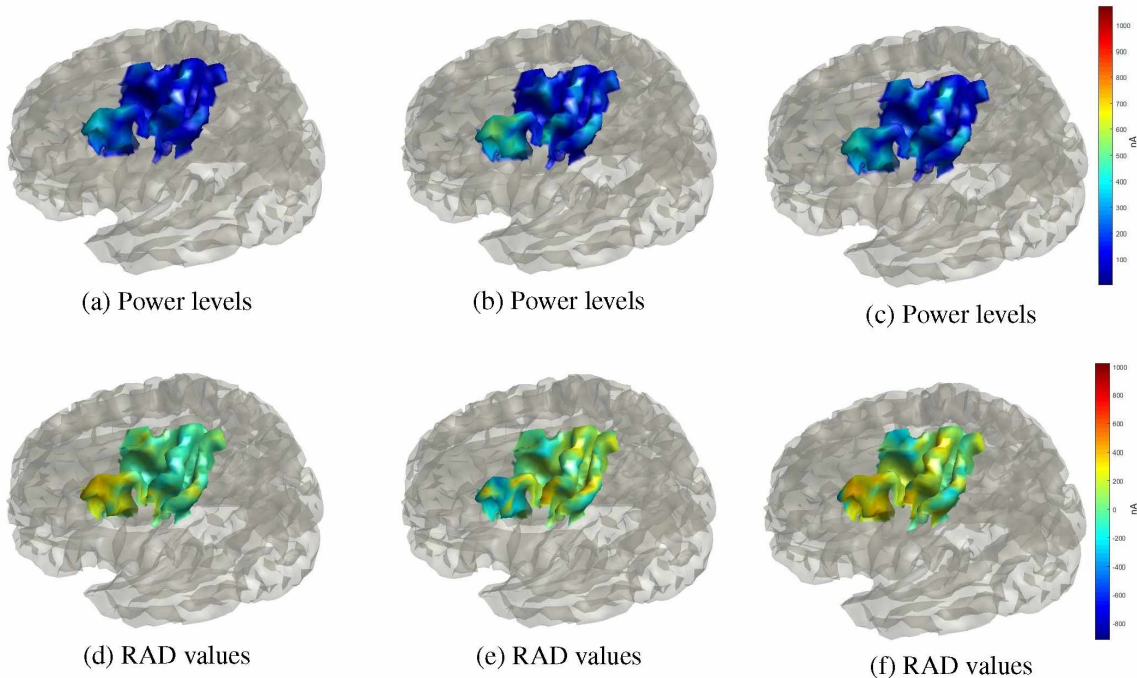


Figure 5.9: CS's RAD and power levels from the onset instant for different wrist pronation movements for a single subject. (a,b,c) Power levels; (d,e,f) RAD values.

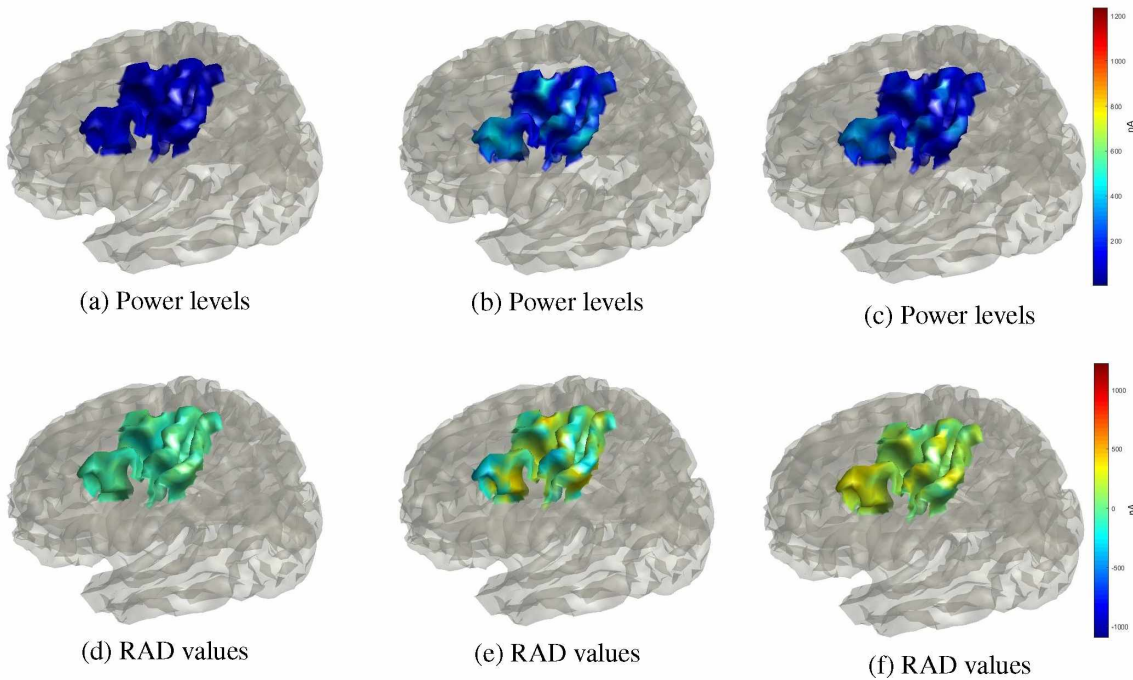


Figure 5.10: CS's RAD and power levels from the onset instant for different elbow extension movements for a single subject. (a,b,c) Power levels; (d,e,f) RAD values.

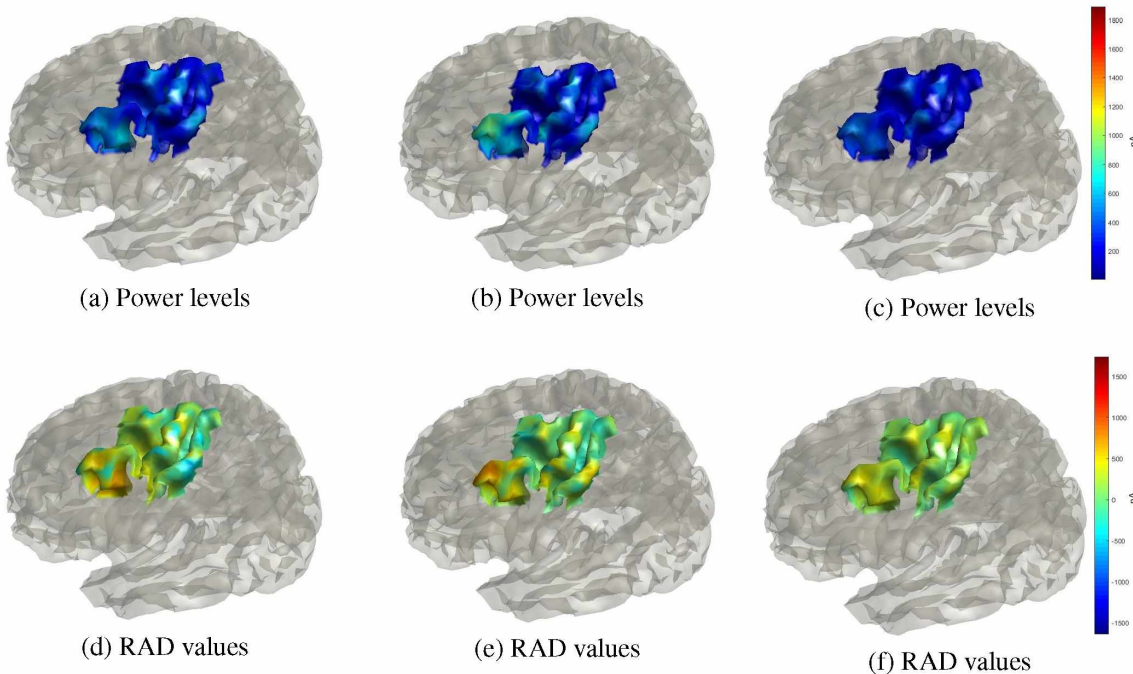


Figure 5.11: CS's RAD and power levels from the onset instant for different elbow flexion movements for a single subject. (a,b,c) Power levels; (d,e,f) RAD values.

this initial analysis, since we are interested in noticing the power fluctuation probably related to *mu* and *beta* frequency rhythms.

Although looking only at the onset moment for every movement class is not enough for in-depth analysis, we can already notice the higher activation in the pre-central and post-central cortices in the majority of cases. This might be due to some variation during the movement performances, but most probably the onset instant is not comparable between movements because of the metric used to find them, or even the signals used for such.

Nonetheless, all of these presented brain signals can be interpreted in accordance to expected behaviour given prior literature knowledge. These signal changes are due to the dynamic between the *mu* and *beta* brain frequency rhythms. These changes can be more easily noticed in the supplementary material, where it is possible to notice a decrease in power levels during movement execution when compared to resting state and position maintenance, according to the knowledge that during movement execution there is a high ERD in the *mu* frequency rhythm (8 to 12 Hz), which usually starts before the movement onset and reaches its maximum shortly after it (NICOLAS-ALONSO; GOMEZ-GIL, 2012). This seems to be the case for the low power levels in Figures 5.6c, 5.7a, 5.7c, 5.8a, 5.8c, 5.9a, 5.10a and 5.11c.

Moreover, it is possible to see high power levels right after movement execution, be it during maintenance or rest state. This is in accordance to the ERS in the *beta* frequency rhythm (12 to 32 Hz), which usually starts right after movement onset and reaches its maximum after movement execution (NICOLAS-ALONSO; GOMEZ-GIL, 2012). This also explains why in some cases there is still some relevant power levels during movement execution, shown in Figures 5.6a, 5.7b, 5.8b, 5.9b, 5.9c, 5.10b, 5.11a and 5.11b.

We can also see the remnant PM activation in Figures 5.6a, 5.6b, 5.7b, 5.8b, 5.9b, 5.9c, 5.10b, 5.11a and 5.11b, which is expected, since this is the brain region related to movement planning and can still be in activation during movement execution (TAYLOR, 1950; HASLINGER *et al.*, 2002).

It is important to highlight that, though EEG has part of all this information, it is not easy see this dynamical signal changes considering a specific activity. Which is understandable, since the considered ROI in this study is directly under only about 8 electrodes (Figure 4.8).

We made an additional visual analysis to reinforce these previous interpretations, taking advantage that there was a section of movements from subject 1 which included all three limb areas (hand, wrist and elbow) one after the other. We calculated the CSs for this whole data segment in order to find differences between the power of each CS during these different movements. Figure 5.12 presents the EEG signals and power levels from CSs inside the ROI for this specific data segment. The signal dynamics over the time grant an easier analysis into the differences between the sub-regions used for controlling each limb area, these are also shown in the supplementary material. However, although different limb areas were activated for each movement, the activated brain sub-regions were very similar, requiring a better analysis approach than simply looking through the power levels.

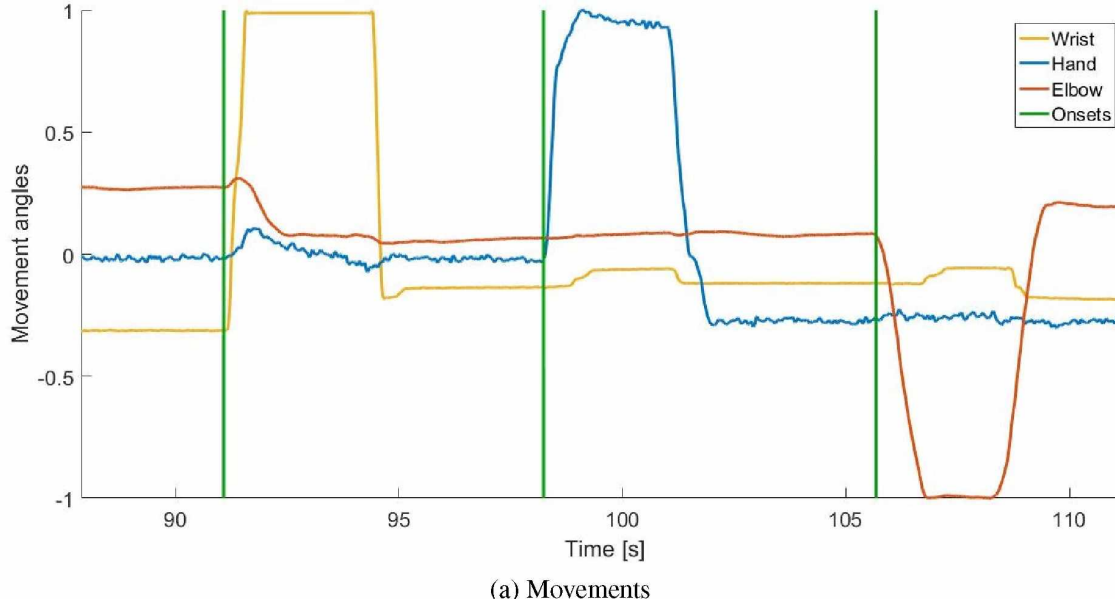
5.2.3 Main related CSs

In order to further investigate the amount of information granted from ESI it would be optimal to investigate each CS, but analysing 491 CSs and interpreting them without the aid of any computational intelligence would be tiresome and time consuming. Therefore, we investigated which were the CSs most relevant during each movement.

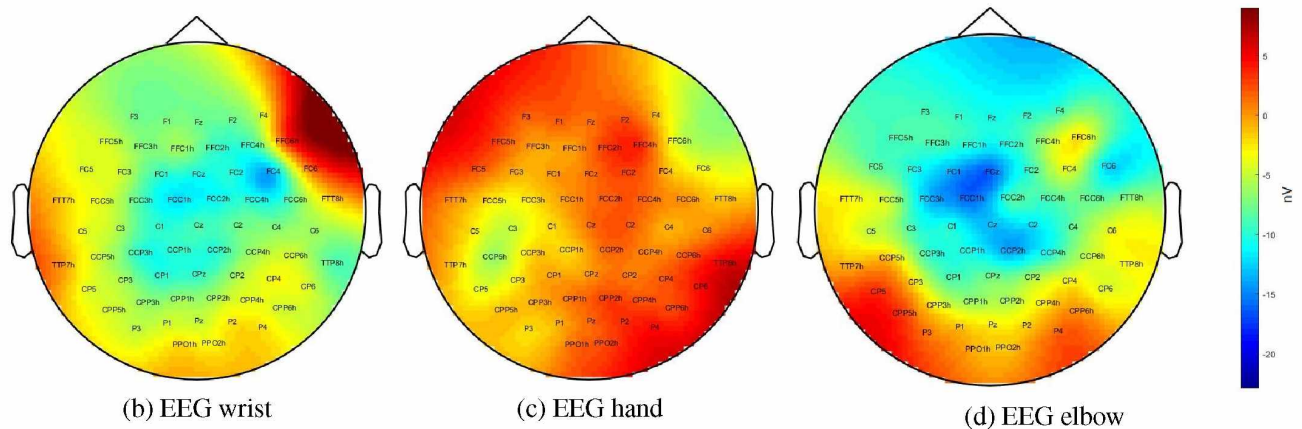
We analysed the changes in power over the *mu* rhythm, and found the CSs consistently considered as relevant among the movements from the same limb region (hand, wrist and elbow). Figure 5.13 shows the CSs, from the ROI presented in fig. 4.7, which were considered as relevant in each movement considering movement planning and execution.

Though the main CSs were different for planning and execution, the strongest ones kept the same in both stages. Therefore, we chose five CSs, as shown in fig. 5.14, for further specific analysis, these were the sources with highest difference for each subregion of our ROI. Therefore, we chose one CS from the S1, one from the upper M1 region (mostly related to wrist and elbow movement), one from the lower M1 region (mostly related to hand movement), one from the dorsal premotor cortex (dPM) and one from the ventral premotor cortex (vPM).

After choosing the most relevant CSs, we can analyse the RAD spectrogram from these to further investigate any expected correlation with the movement itself. We chose to only focus in the



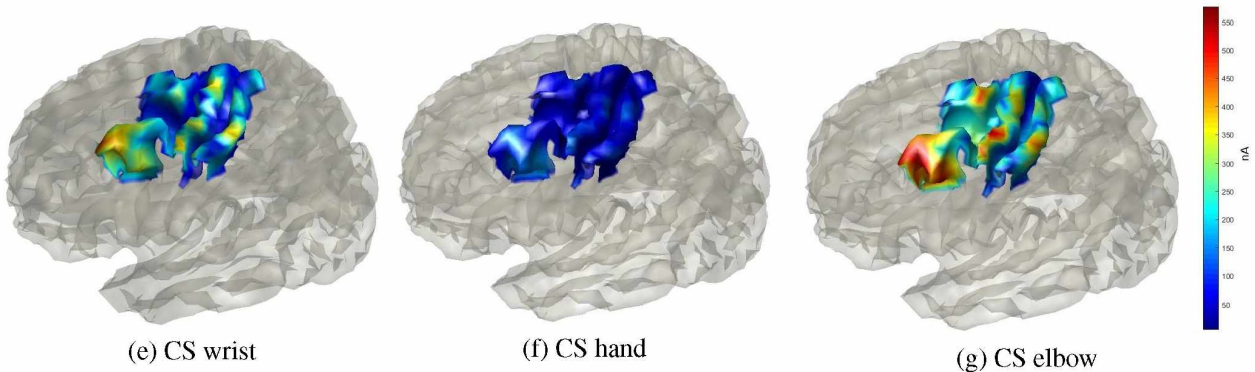
(a) Movements



(b) EEG wrist

(c) EEG hand

(d) EEG elbow



(e) CS wrist

(f) CS hand

(g) CS elbow

Figure 5.12: CS power levels and EEG topographic analysis during different movements for a single subject in a continuous segment. (a) Limb positions from data glove and exoskeleton for wrist (blue), hand (red) and elbow (yellow) movement and a cursor (green) indicating the time sample for each of the following sub-figures respectively; (b, c and d) EEG topographic analysis during wrist, hand and elbow movements respectively; (e, f and g) CS power levels during wrist hand and elbow movements respectively.

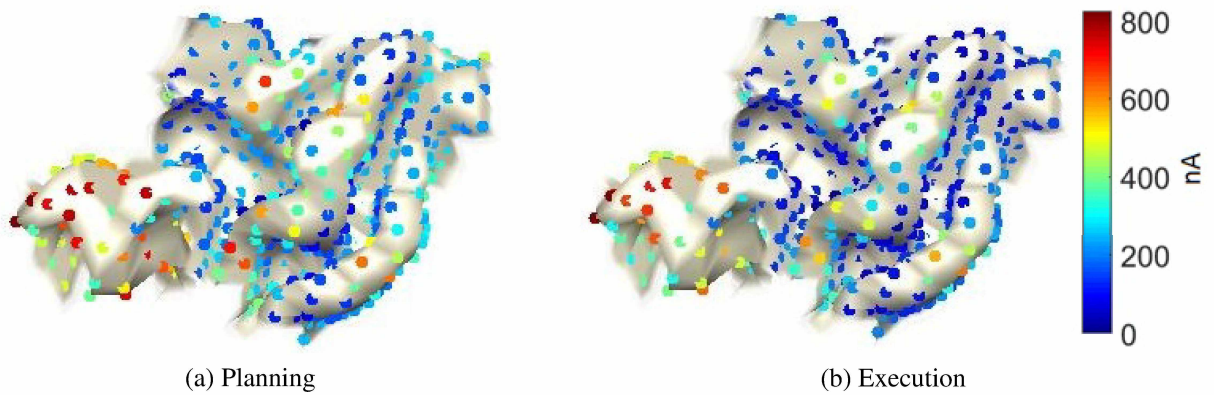


Figure 5.13: CSs from the ROI considered as most relevant for hand movement (between before and during motor planning: a; and between motor planning and execution: b). Point colors indicate the level of *mu* power difference for each CS.

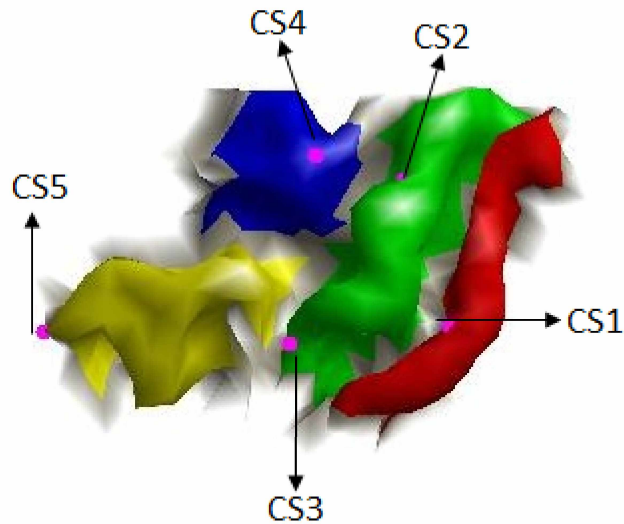


Figure 5.14: CSs considered for time and frequency analysis in magenta. Surface colors indicate brain sub-regions: vPM (yellow); dPM (blue); M1 (green); and S1 (red).

frequency range between 4 and 36 Hz since these are most prominent in EEG signals. Figures 5.15 to 5.17 show some behavioural difference among brain regions regarding a frequency analysis in the CSs considered as mainly related to the movement executions. In them we can see a high similarity between the signals, which is understandable given their location and possible connection (HÄMÄLÄINEN *et al.*, 1993).

Nonetheless, there are distinctive differences among them. For instance, there is a slight delay between activation from PM CSs to M1 CSs and from M1 CSs to S1 CSs. Moreover, it is

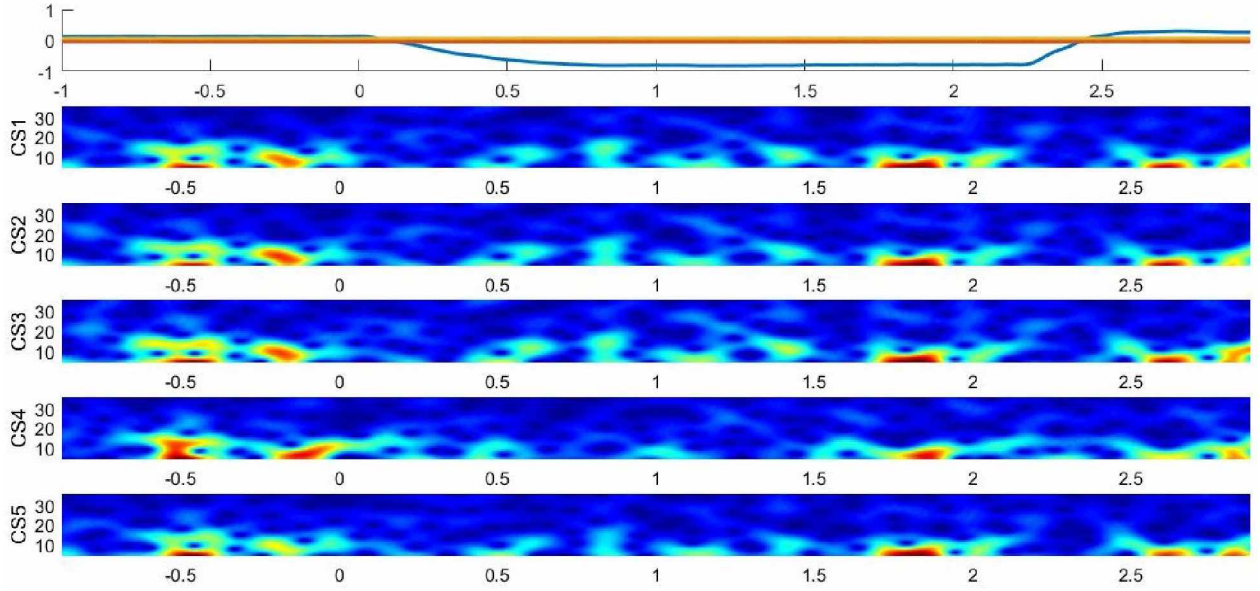


Figure 5.15: Limb positions during hand movement from subject 1 presented along with the spectrogram of the five specific CSs considered as relevant. Color values are from dark blue (lowest) to dark red (highest).

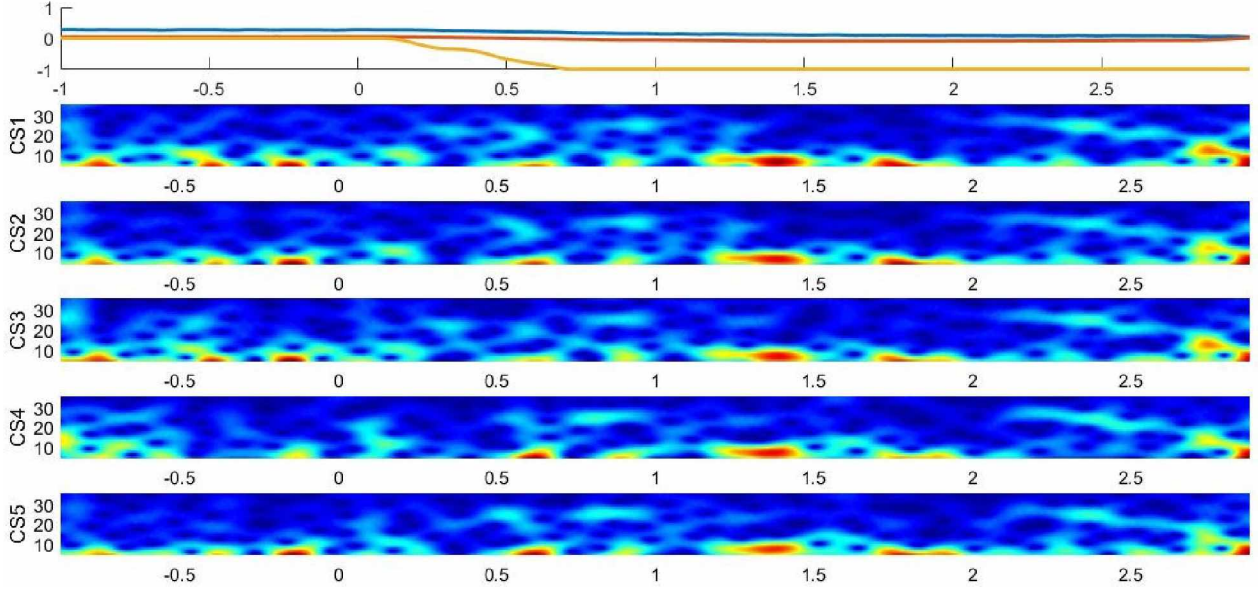


Figure 5.16: Limb positions during wrist movement from subject 1 presented along with the spectrogram of the five specific CSs considered as relevant. Color values are from dark blue (lowest) to dark red (highest).

also easy to see the ERS in the mu rhythm during movement execution for the three movement regions (hand, wrists and elbow).

Yet, the most relevant analysis that we can make is comparing the two CSs from the M1. For the hand movement (fig. 5.15), we notice overall higher activation levels in the CS closer

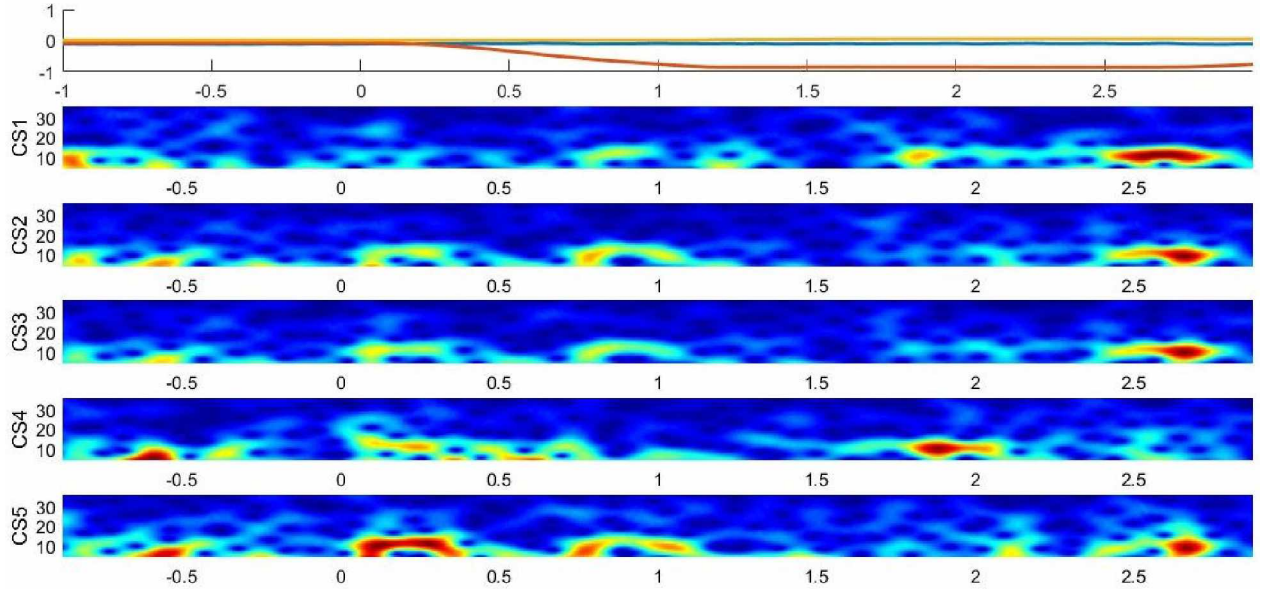


Figure 5.17: Limb positions during elbow movement from subject 1 presented along with the spectrogram of the five specific CSs considered as relevant. Color values are from dark blue (lowest) to dark red (highest).

to the hand-related region, while for elbow movement (fig. 5.17), we notice these overall higher activation levels in the CS closer to elbow the elbow-related region (PURVES *et al.*, 2004). For the wrist movement (fig. 5.16), we did not notice much visual difference between the two.

We can also investigate differences considering the same movement as seen in Figures 5.18 to 5.20, which show the RAD spectrogram from the chosen CSs (fig. 5.14) during hand, wrist and elbow movements from subject 1 respectively. While these differences might carry relevant dynamical information regarding speed, position or acceleration, these assumptions would require a data set which can more reliably analyse such differences. Yet the consistency maintains in that the previous analysis derived from figs. 5.15 to 5.17 are still present in all these other spectrograms.

These specific CS analyses are further proof that the information from ESI is in accordance to the signal dynamic (mainly considering mu and beta rhythms) so far presented in the literature. We mainly considered visual differences, but if used along with robust classifiers, maybe even more information can be extracted from ESI, like direction and speed (RICKERT *et al.*, 2005; NAKANISHI *et al.*, 2017). However, the used data set is not optimal for these analyses. Rather, we were able to easily see differences between the limb areas which were activated, showing the applicability of ESI for classifying between these, and even differentiating the movements given

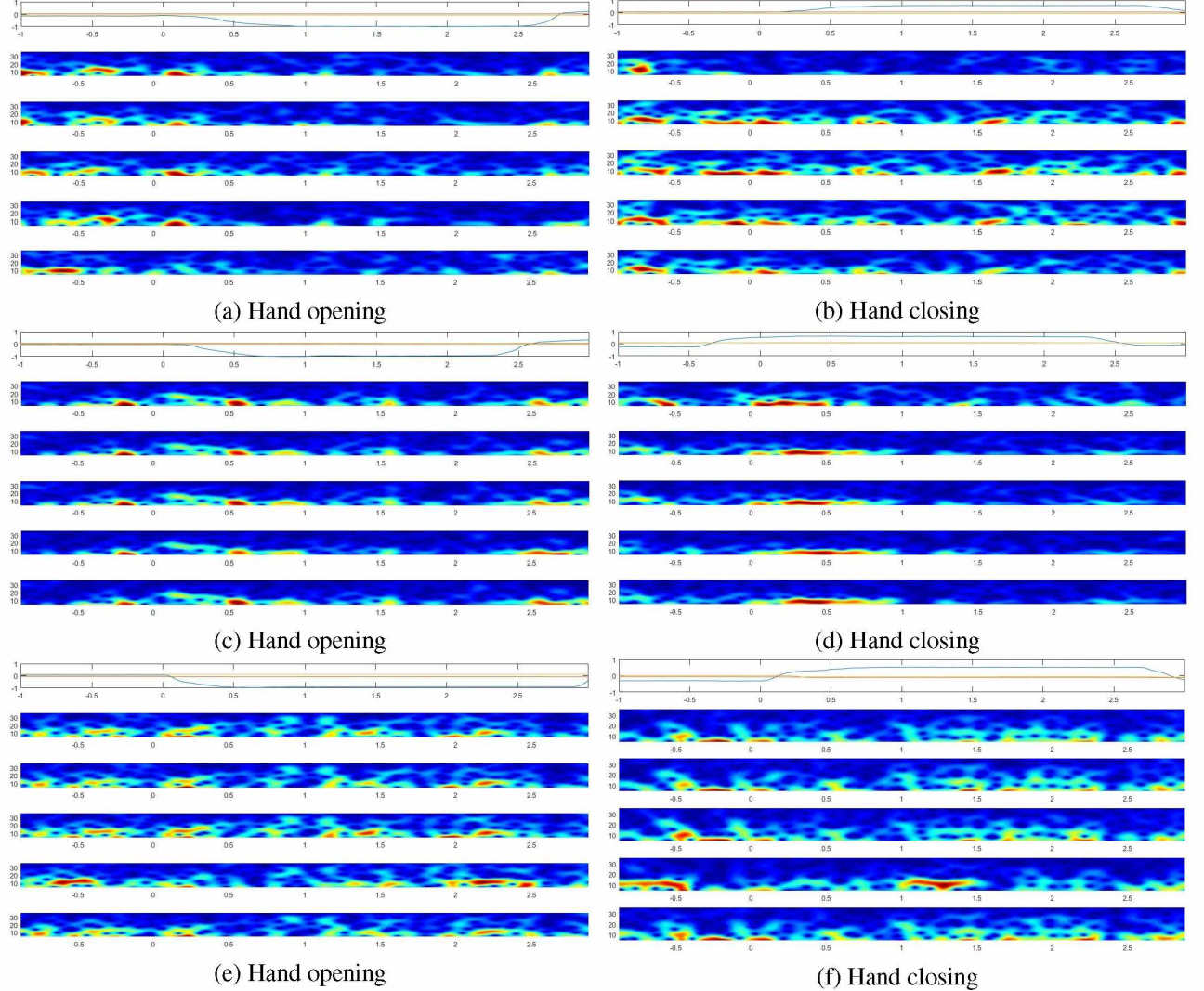


Figure 5.18: Limb positions during hand opening and closing movements from subject 1 presented along with the spectrogram of the five specific CSs considered as relevant presented from top to bottom (CS1 to CS5). Color values are from dark blue (lowest) to dark red (highest).

the dynamical differences which can be easily seen considering the same movement (figs. 5.18 to 5.20).

It is noteworthy that there is a great variation between signals even from the same movement type. These variations should be because of other brain activities happening at the same time as the movement execution or even changes in the details of said execution. Again, this gives margin to speculate that there is more retrievable information from the brain when reading the EEG

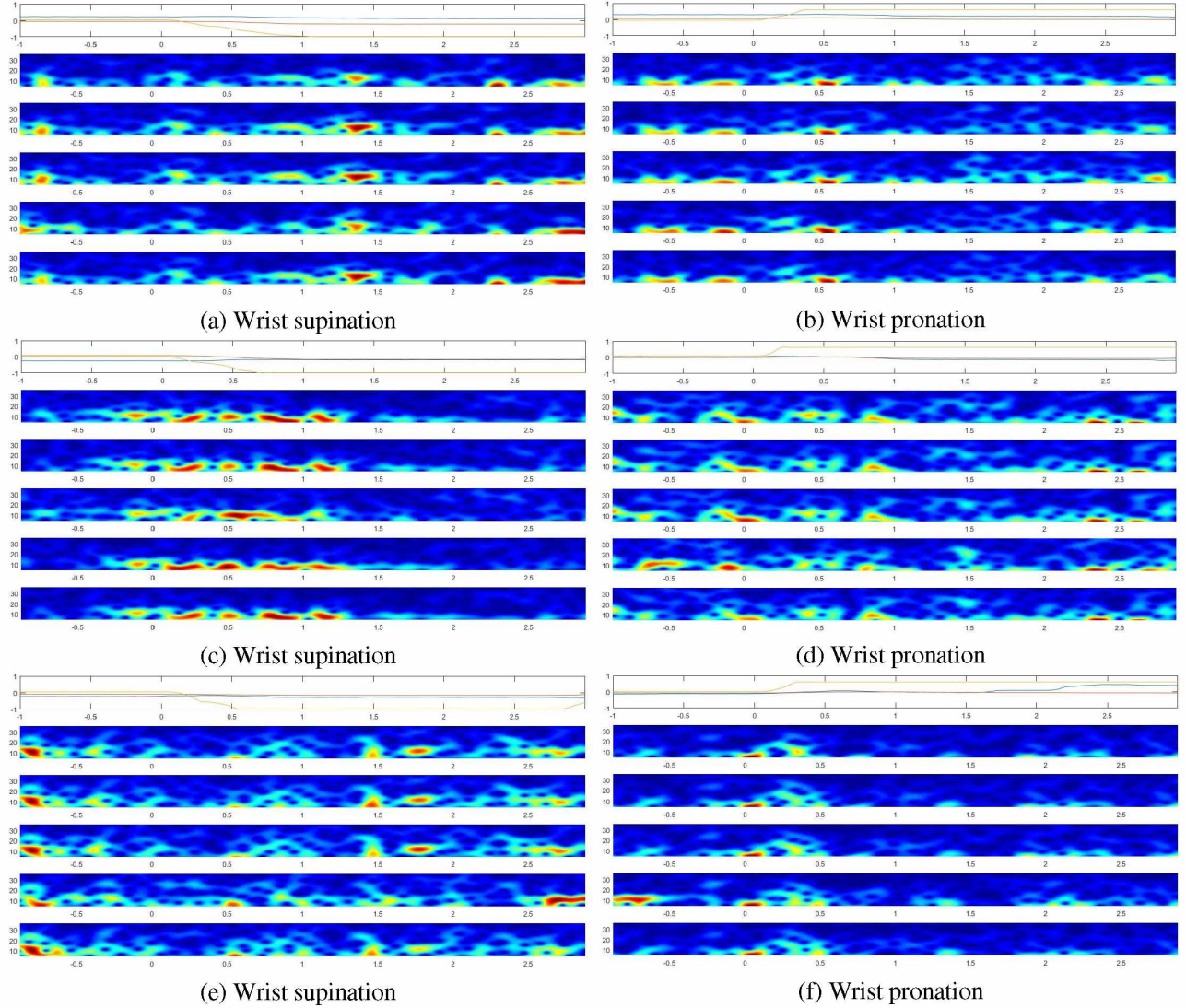


Figure 5.19: Limb positions during wrist supination and pronation movements from subject 1 presented along with the spectrogram of the five specific CSs considered as relevant presented from top to bottom (CS1 to CS5). Color values are from dark blue (lowest) to dark red (highest).

signals with added spatial information through ESI. Therefore, the spacial information addition is noteworthy and can be highly reliable for applications which include brain signal interpretation such as brain machine interfaces.

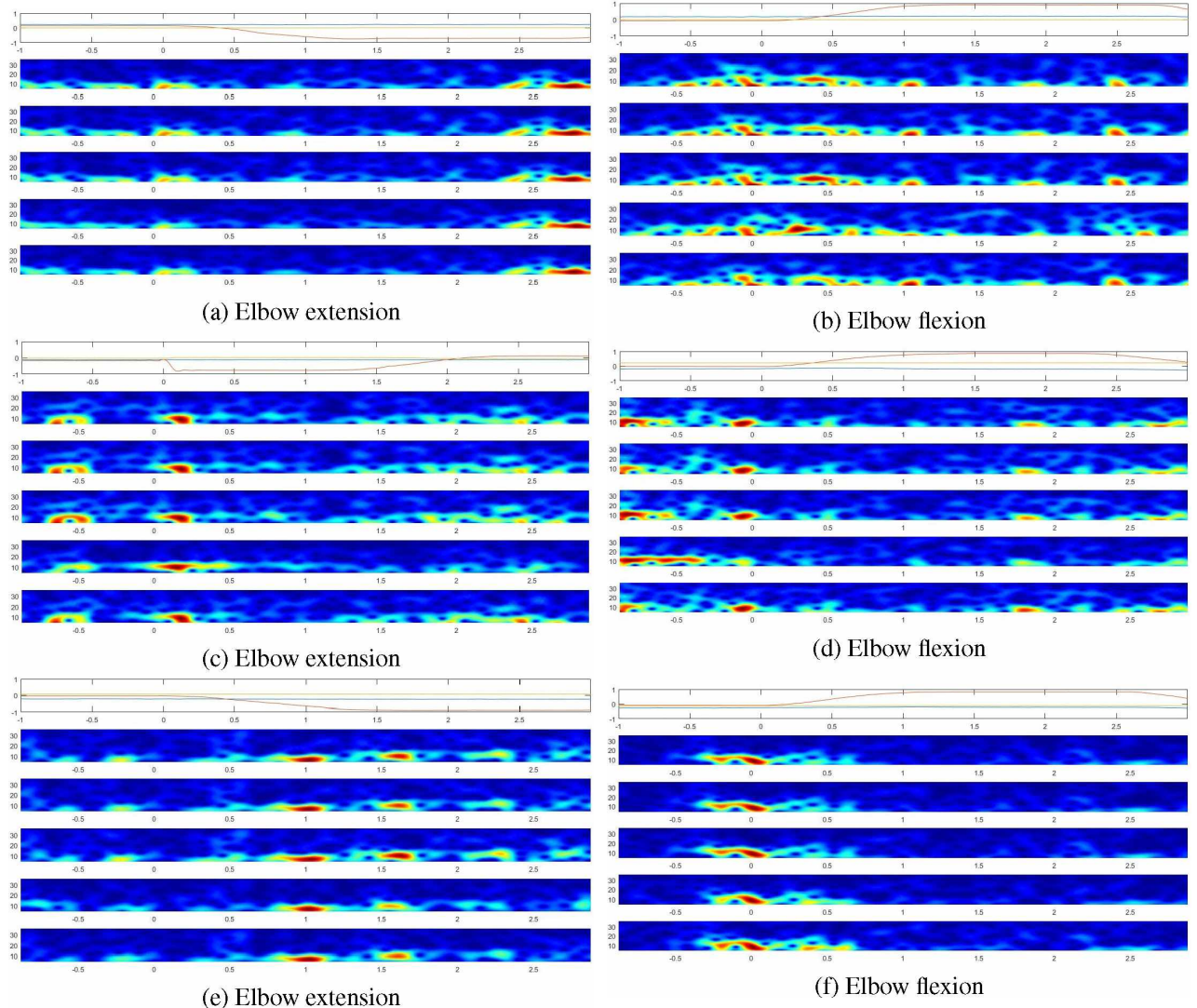


Figure 5.20: Limb positions during elbow extension and flexion movements from subject 1 presented along with the spectrogram of the five specific CSs considered as relevant presented from top to bottom (CS1 to CS5). Color values are from dark blue (lowest) to dark red (highest).

6 CONCLUSION

We proposed to prove with this study that the use of ESI might provide more specific information during movements from different parts of the same limb, allowing for a better differentiation between those, even allowing for a deep analysis of the regions and signals related to these movements.

The main goal was to verify a significant and consistent difference on signals from hand, wrist and elbow movements by applying ESI to an EEG data set. If these differences were in accordance to prior literature knowledge, then our hypothesis is assured.

We separated the whole process into two main stages: Validation and Application. In the validation stage we verified the performance and reliability of the chosen ESI method using simulated data in different settings and even real data.

In the application stage we applied the previously validated ESI method to a sampled EEG data set on which the subjects performed hand, wrist and elbow movements. We then analysed the internal current source (CS) signals to find an expected behavior when compared to the literature. We also applied a dimension reduction technique based on the expected signal behavior to find the most relevant CSs inside the brain region mostly related to these movements. With these specific CSs we were able to analyze their time-frequency behavior using spectrograms.

The chosen ESI method (eLORETA) was correctly validated and granted a considerable spatial resolution increase in the application stage: from 61 electrodes (approximately 24.69 mm apart) to 8196 CSs (approximately 3.67 mm apart). The time-frequency behavior of the CSs in general and in specific is in accordance to the literature when considering the power fluctuations in *mu* and *beta* rhythms during movement planning and execution. The results also showed differences between the movements in regards to signal behavior, but mostly difference between single CS behavior as expected, since there are brain regions more specifically related to each of the limb regions of these movements.

The results show the applicability of eLORETA for analysing movement related brain signals, once it grants a spatial resolution increase which is reliable and coherent with the literature. This opens ground for enhancing further studies, for example, using eLORETA for enhancing the

quality of brain machine interfaces. However, it also opens for the study of applying other ESI models and enhance this application in other aspects such as computational effort as well as more signal precision.

There are many improvements to be done in the field, but we prove in this study that there is substantial reason to apply ESI on brain studies when possible, given its increase in information.

6.1 Future works

There are more investigations to be made regarding the application of ESI in motor control of a single limb. Therefore, we propose these future works:

- Implement different ESI mathematical methods, and generate a more advanced simulation protocol for validation.
- Use a computational classifier for objectively differentiating between the studied movements in this study and compare its performance using standard EEG features in comparison to using ESI features for the classification;
- Apply a similar study in order to differentiate between movements from even closer brain regions such as different finger motion from the same hand;
- Develop a more specific protocol for data acquisition which can be further used for investigation of dynamical movement information such as changes in position, velocity and acceleration.

BIBLIOGRAPHY

- BALL, T.; SCHREIBER, A.; FEIGE, B.; WAGNER, M.; LÜCKING, C. H.; KRISTEVA-FEIGE, R. The Role of Higher-Order Motor Areas in Voluntary Movement as Revealed by High-Resolution EEG and fMRI. *NeuroImage*, n. 6, p. 682–694, 1999. ISSN 10538119. Disponível em: <<https://doi.org/10.1006/nimg.1999.0507>>.
- BLEICHNER, M. G.; JANSMA, J. M.; SELLMEIJER, J.; RAEMAEKERS, M.; RAMSEY, N. F. Give me a sign: Decoding complex coordinated hand movements using high-field fMRI. *Brain Topography*, v. 27, n. 2, p. 248–257, 2014. ISSN 08960267. Disponível em: <<https://doi.org/10.1007/s10548-013-0322-x>>.
- BOONSTRA, T. W.; DAFFERTSHOFER, A.; BREAKSPEAR, M.; BEEK, P. J. Multivariate time-frequency analysis of electromagnetic brain activity during bimanual motor learning. *NeuroImage*, Elsevier Inc., v. 36, n. 2, p. 370–377, 2007. ISSN 10538119. Disponível em: <<http://dx.doi.org/10.1016/j.neuroimage.2007.03.012>>.
- BRODBECK, V.; LASCANO, A. M.; SPINELLI, L.; SEECK, M.; MICHEL, C. M. Accuracy of EEG source imaging of epileptic spikes in patients with large brain lesions. *Clinical Neurophysiology*, International Federation of Clinical Neurophysiology, v. 120, n. 4, p. 679–685, 2009. ISSN 13882457. Disponível em: <<http://dx.doi.org/10.1016/j.clinph.2009.01.011>>.
- BUNDY, D. T.; PAHWA, M.; SZRAMA, N.; LEUTHARDT, E. C. Decoding three-dimensional reaching movements using electrocorticographic signals in humans. *Journal of neural engineering*, IOP Publishing, v. 13, n. 2, p. 026021, 2016. ISSN 1741-2552. Disponível em: <<https://doi.org/10.1088/1741-2560/13/2/026021>>.
- COITO, A.; MICHEL, C. M.; Van Mierlo, P.; VULLIEMOZ, S.; PLOMP, G. Directed Functional Brain Connectivity Based on EEG Source Imaging: Methodology and Application to Temporal Lobe Epilepsy. *IEEE Transactions on Biomedical Engineering*, v. 63, n. 12, p. 2619–2628, 2016. ISSN 15582531. Disponível em: <<https://doi.org/10.1109/TBME.2016.2619665>>.
- CORDELLA, F.; CIANCIO, A. L.; SACCHETTI, R.; DAVALLI, A.; CUTTI, A. G.; GUGLIELMELLI, E.; ZOLLO, L. Literature review on needs of upper limb prosthesis users. *Frontiers in Neuroscience*, v. 10, n. MAY, p. 1–14, 2016. ISSN 1662453X.
- COSTA, F.; BATATIA, H.; OBERLIN, T.; GIANO, C. D.; TOURNERET, J.-y. NeuroImage Bayesian EEG source localization using a structured sparsity prior. *NeuroImage*, v. 144, p. 142–152, 2017. ISSN 1053-8119. Disponível em: <<http://dx.doi.org/10.1016/j.neuroimage.2016.08.064>>.
- CUSTO, A.; VULLIEMOZ, S.; GROUILLER, F.; Van De Ville, D.; MICHEL, C. EEG source imaging of brain states using spatiotemporal regression. *NeuroImage*, Elsevier Inc., v. 96, p.

- 106–116, 2014. ISSN 10959572. Disponível em: <<http://dx.doi.org/10.1016/j.neuroimage.2014.04.002>>.
- EDELMAN, B.; BAXTER, B.; HE, B. Decoding and mapping of right hand motor imagery tasks using EEG source imaging. *2015 7th International IEEE/EMBS Conference on Neural Engineering (NER)*, p. 194–197, 2015. ISSN 1948-3546. Disponível em: <<http://ieeexplore.ieee.org/lpdocs/epic03/wrapper.htm?arnumber=7146593>>.
- EDELMAN, B. J.; BAXTER, B.; HE, B. EEG source imaging enhances the decoding of complex right-hand motor imagery tasks. *IEEE Transactions on Biomedical Engineering*, v. 63, n. 1, p. 4–14, 2016. ISSN 15582531.
- FONOV, V.; EVANS, A. C.; BOTTERON, K.; ALMLI, C. R.; MCKINSTRY, R. C.; COLLINS, D. L. Unbiased average age-appropriate atlases for pediatric studies. *NeuroImage*, Elsevier Inc., v. 54, n. 1, p. 313–327, 2011. ISSN 10538119. Disponível em: <<http://dx.doi.org/10.1016/j.neuroimage.2010.07.033>>.
- FUCHS, M.; FORD, M. R.; SANDS, S.; LEW, H. L. Overview of dipole source localization. *Physical Medicine and Rehabilitation Clinics of North America*, v. 15, n. 1, p. 251–262, 2004. ISSN 10479651. Disponível em: <[https://doi.org/10.1016/S1047-9651\(03\)00126-8](https://doi.org/10.1016/S1047-9651(03)00126-8)>.
- GERARDIN, E.; POCHON, J. B.; POLINE, J. B.; TREMBLAY, L.; Van De Moortele, P. F.; LEVY, R.; DUBOIS, B.; Le Bihan, D.; LEHÉRICY, S. Distinct striatal regions support movement selection, preparation and execution. *NeuroReport*, v. 15, n. 15, p. 2327–2331, 2004. ISSN 09594965. Disponível em: <<https://doi.org/10.1097/00001756-200410250-00005>>.
- GRAMFORT, A.; LUSSI, M.; LARSON, E.; ENGEMANN, D. A.; STROHMEIER, D.; BRODBECK, C.; GOJ, R.; JAS, M.; BROOKS, T.; PARKKONEN, L.; HÄMÄLÄINEN, M. MEG and EEG data analysis with MNE-Python. *Frontiers in Neuroscience*, v. 7, n. 7 DEC, p. 1–13, 2013. ISSN 1662453X.
- GRECH, R.; CASSAR, T.; MUSCAT, J.; CAMILLERI, K. P.; FABRI, S. G.; ZERVAKIS, M.; XANTHOPOULOS, P.; SAKKALIS, V.; VANRUMSTE, B. Review on solving the inverse problem in EEG source analysis. *Journal of NeuroEngineering and Rehabilitation*, v. 5, p. 1–33, 2008. ISSN 17430003.
- GUNASEKERA, B.; SAXENA, T.; BELLAMKONDA, R.; KARUMBAIAH, L. Intracortical recording interfaces: Current challenges to chronic recording function. *ACS Chemical Neuroscience*, v. 6, n. 1, p. 68–83, 2015. ISSN 19487193.
- HALLEZ, H.; VANRUMSTE, B.; GRECH, R.; MUSCAT, J.; De Clercq, W.; VERGULT, A.; D'ASSELER, Y.; CAMILLERI, K. P.; FABRI, S. G.; Van Huffel, S.; LEMAHIEU, I. *Review on solving the forward problem in EEG source analysis*. 2007.
- HÄMÄLÄINEN, M.; HARI, R.; ILMONIEMI, R. J.; KNUUTILA, J.; LOUNASMAA, O. V. Magnetoencephalography theory, instrumentation, and applications to noninvasive studies of the

working human brain. *Reviews of Modern Physics*, v. 65, n. 2, p. 413–497, 1993. ISSN 00346861. Disponível em: <<https://doi.org/10.1103/RevModPhys.65.413>>.

HÄMÄLÄINEN, M. S.; ILMONIEMI, R. J. Interpreting magnetic fields of the brain: minimum norm estimates. *Medical & Biological Engineering & Computing*, v. 32, n. 1, p. 35–42, 1994. ISSN 01400118. Disponível em: <<https://doi.org/10.1007/BF02512476>>.

HASLINGER, B.; ERHARD, P.; WEILKE, F.; EINSIEDEL, V.; SCHWAIGER, M.; CONRAD, B.; BARTENSTEIN, P.; GRAFIN, H. The role of lateral premotor – cerebellar – parietal circuits in motor sequence control : a parametric fMRI study. v. 13, p. 159–168, 2002. Disponível em: <[https://doi.org/10.1016/S0926-6410\(01\)00104-5](https://doi.org/10.1016/S0926-6410(01)00104-5)>.

HASSAN, M.; DUFOR, O.; MERLET, I.; BERROU, C.; WENDLING, F. EEG source connectivity analysis: From dense array recordings to brain networks. *PLoS ONE*, v. 9, n. 8, 2014. ISSN 19326203. Disponível em: <<https://doi.org/10.1371/journal.pone.0105041>>.

HAUFE, S.; TOMIOKA, R.; DICKHAUS, T.; SANNELLI, C.; BLANKERTZ, B.; NOLTE, G.; MÜLLER, K. R. Large-scale EEG/MEG source localization with spatial flexibility. *NeuroImage*, Elsevier Inc., v. 54, n. 2, p. 851–859, 2011. ISSN 10538119. Disponível em: <<http://dx.doi.org/10.1016/j.neuroimage.2010.09.003>>.

JAIR MONTOYA MARTÍNEZ. Functional Brain Imaging on Mobile Devices By Solving the Eeg Inverse Problem: a Structured Sparsity Approach. *Igarss 2014*, n. 1, p. 1–5, 2014. ISSN 13514180.

JATOI, M. A.; KAMEL, N.; MALIK, A. S.; FAYE, I.; BEGUM, T. A survey of methods used for source localization using EEG signals. *Biomedical Signal Processing and Control*, Elsevier Ltd, v. 11, n. 1, p. 42–52, 2014. ISSN 17468108. Disponível em: <<http://dx.doi.org/10.1016/j.bspc.2014.01.009>>.

JERBI, K.; VIDAL, J. R.; MATTOUT, J.; MABY, E.; LECAIGNARD, F.; OSSANDON, T.; HAMAMÉ, C. M.; DALAL, S. S.; BOUET, R.; LACHAUX, J. P.; LEAHY, R. M.; BAILLET, S.; GARNERO, L.; DELPUECH, C.; BERTRAND, O. Inferring hand movement kinematics from MEG, EEG and intracranial EEG: From brain-machine interfaces to motor rehabilitation. *Irbm*, Elsevier Masson SAS, v. 32, n. 1, p. 8–18, 2011. ISSN 19590318. Disponível em: <<http://dx.doi.org/10.1016/j.irbm.2010.12.004>>.

KAO, J. C.; NYUJUKIAN, P.; RYU, S. I.; CHURCHLAND, M. M.; CUNNINGHAM, J. P.; SHENOY, K. V. Single-trial dynamics of motor cortex and their applications to brain-machine interfaces. *Nature Communications*, Nature Publishing Group, v. 6, n. May, p. 1–12, 2015. ISSN 20411723. Disponível em: <<http://dx.doi.org/10.1038/ncomms8759>>.

KATO, S.; KAPLAN, H. S.; SCHRÖDEL, T.; SKORA, S.; LINDSAY, T. H.; YEMINI, E.; LOCKERY, S.; ZIMMER, M. Global Brain Dynamics Embed the Motor Command Sequence of *Caenorhabditis elegans*. *Cell*, v. 163, n. 3, p. 656–669, 2015. ISSN 10974172. Disponível em: <<https://doi.org/10.1016/j.cell.2015.09.034>>.

- KIMURA, M.; OHIRA, H.; SCHRÖGER, E. Localizing sensory and cognitive systems for pre-attentive visual deviance detection: An sLORETA analysis of the data of Kimura et al. (2009). *Neuroscience Letters*, v. 485, n. 3, p. 198–203, 2010. ISSN 03043940. Disponível em: <<https://doi.org/10.1016/j.neulet.2010.09.011>>.
- KOCAK, M.; ULMER, J. L.; UGUREL, M. S.; GAGGL, W.; PROST, R. W. Motor homunculus: Passive mapping in healthy volunteers by using functional MR imaging - Initial results. *Radiology*, v. 251, n. 2, p. 485–492, 2009. ISSN 00338419. Disponível em: <<https://doi.org/10.1007/s12392-009-0202-7>>.
- KOHLER, T.; WAGNER, M.; FUCHS, M.; WISCHMANN, H. A.; DRENCKHAHN, R.; THEISSEN, A. Depth normalization in MEG/EEG current density imaging. *IEEE Engineering in Medicine and Biology Society, 18th Annual International Conference*, p. 812–813, 1996. ISSN 1687-5273.
- LEE, K. M.; CHANG, K. H.; ROH, J. K. Subregions within the supplementary motor area activated at different stages of movement preparation and execution. *NeuroImage*, v. 9, n. 1, p. 117–123, 1999. ISSN 10538119.
- LEEB, R.; TONIN, L.; ROHM, M.; DESIDERI, L.; CARLSON, T.; MILLÁN, J. D. R. Towards independence: A BCI telepresence robot for people with severe motor disabilities. *Proceedings of the IEEE*, v. 103, n. 6, p. 969–982, 2015. ISSN 00189219.
- LEO, A.; HANDJARAS, G.; BIANCHI, M.; MARINO, H.; GABICCINI, M.; GUIDI, A.; SCILINGO, E. P.; PIETRINI, P.; BICCHI, A.; SANTELLO, M.; RICCIARDI, E. A synergy-based hand control is encoded in human motor cortical areas. *eLife*, v. 5, n. FEBRUARY2016, p. 1–32, 2016. ISSN 2050084X. Disponível em: <<https://doi.org/10.7554/eLife.13420>>.
- LOTTE, F.; CONGEDO, M.; LÉCUYER, a.; LAMARCHE, F.; ARNALDI, B. A review of classification algorithms for EEG-based ;computer interfaces. *Journal of Neural Engineering*, v. 4, n. 2, p. R1–R13, 2007. ISSN 17412552.
- MAHJOORY, K.; NIKULIN, V. V.; BOTREL, L.; LINKENKAER-HANSEN, K.; FATO, M. M.; HAUFE, S. Consistency of EEG source localization and connectivity estimates. *NeuroImage*, Elsevier, v. 152, n. February, p. 590–601, 2017. ISSN 10959572. Disponível em: <<http://dx.doi.org/10.1016/j.neuroimage.2017.02.076>>.
- MAYHEW, S. D.; PORCARO, C.; TECCHIO, F.; BAGSHAW, A. P. fMRI characterisation of widespread brain networks relevant for behavioural variability in fine hand motor control with and without visual feedback. *NeuroImage*, Elsevier, v. 148, n. June 2016, p. 330–342, 2017. ISSN 10959572. Disponível em: <<http://dx.doi.org/10.1016/j.neuroimage.2017.01.017>>.
- MAZZIOTTA, J. C.; TOGA, A. W.; EVANS, A.; FOX, P.; LANCASTER, J. *A probabilistic atlas of the human brain: theory and rationale for its development. The International Consortium for Brain Mapping (ICBM)*. 1995. 89–101 p.

- MCFARLAND, D. J.; MINER, L. A.; VAUGHAN, T. M.; WOLPAW, J. R. Mu and beta rhythm topographies during motor imagery and actual movements. *Brain Topography*, v. 12, n. 3, p. 177–186, 2000. ISSN 08960267.
- MICHEL, C. M.; MURRAY, M. M.; LANTZ, G.; GONZALEZ, S.; SPINELLI, L.; Grave De Peralta, R. EEG source imaging. *Clinical Neurophysiology*, v. 115, n. 10, p. 2195–2222, 2004. ISSN 13882457. Disponível em: <<https://doi.org/10.1016/j.clinph.2004.06.001>>.
- MIDDLETON, F. A.; STRICK, P. L. Basal ganglia and cerebellar loops: Motor and cognitive circuits. *Brain Research Reviews*, v. 31, n. 2-3, p. 236–250, 2000. ISSN 01650173. Disponível em: <[https://doi.org/10.1016/S0165-0173\(99\)00040-5](https://doi.org/10.1016/S0165-0173(99)00040-5)>.
- MUKAKA, M. M. 81576-194640-1-Pb. *Malawi Medical Journal*, v. 24, n. September, p. 69–71, 2012. ISSN 1995-7270. Disponível em: <<https://www.ajol.info/index.php/mmj/article/view/81576>>.
- NAKANISHI, Y.; YANAGISAWA, T.; SHIN, D.; KAMBARA, H.; YOSHIMURA, N.; TANAKA, M.; FUKUMA, R.; KISHIMA, H.; HIRATA, M.; KOIKE, Y. Mapping ECoG channel contributions to trajectory and muscle activity prediction in human sensorimotor cortex. *Scientific Reports*, Nature Publishing Group, v. 7, n. October 2016, p. 45486, 2017. ISSN 2045-2322. Disponível em: <<http://dx.doi.org/10.1038/srep45486><http://www.nature.com/articles/srep45486>>.
- NAM, S.; KIM, D.-S. Reconstruction of Arm Movement Directions from Human Motor Cortex Using fMRI. *Frontiers in Neuroscience*, v. 11, n. July, 2017. ISSN 1662-453X. Disponível em: <<http://journal.frontiersin.org/article/10.3389/fnins.2017.00434/full>>.
- NICOLAS-ALONSO, L. F.; GOMEZ-GIL, J. Brain computer interfaces, a review. *Sensors*, v. 12, n. 2, p. 1211–1279, 2012. ISSN 14248220. Disponível em: <<https://doi.org/10.3390/s120201211>>.
- OFNER, P.; SCHWARZ, A.; PEREIRA, J.; MÜLLER-PUTZ, G. R. Upper limb movements can be decoded from the time-domain of low-frequency EEG. *PLoS ONE*, v. 12, n. 8, p. 1–24, 2017. ISSN 19326203.
- OOSTENVELD, R.; FRIES, P.; MARIS, E.; SCHOFFELEN, J. M. FieldTrip: Open source software for advanced analysis of MEG, EEG, and invasive electrophysiological data. *Computational Intelligence and Neuroscience*, v. 2011, 2011. ISSN 16875265. Disponível em: <<https://doi.org/10.1155/2011/674605>>.
- PASCUAL-MARQUI, R. D. Reply to comments made by R. Grave De Peralta Menendez and S.L. Gozalez Adino. *International Journal of Bioelectromagnetism*, v. 1, n. 2, p. 1–10, 1999. Disponível em: <<http://www.uzh.ch/keyinst/NewLORETA/SomePapers/LORETAcv/01-Reply.pdf>>.
- PASCUAL-MARQUI, R. D. Standardized low-resolution brain electromagnetic tomography (sLORETA): technical details. *Methods and findings in experimental and clinical pharmacology*, v. 24 Suppl D, p. 5–12, 2002. ISSN 0379-0355.

PURVES, D.; AUGUSTINE, G. J.; FITZPATRICK, D.; HALL, W. C.; LAMANTIA, A.-S.; MCNAMARA, J. O.; WILLIAMS, S. M. (Ed.). *Neuroscience*. Third edition. Sunderland, Massachusetts USA: Sinauer Associates, Inc, 2004.

RANADE, G. V.; GANGULY, K.; CARMENA, J. LFP beta power predicts cursor stationarity in BMI task. *2009 4th International IEEE/EMBS Conference on Neural Engineering, NER '09*, IEEE, p. 482–485, 2009.

RICKERT, J.; Cardoso De Oliveira, S.; VAADIA, E.; AERTSEN, A.; ROTTER, S.; MEHRING, G. Encoding of movement direction in different frequency ranges of motor cortical local field potentials. *Journal of Neuroscience*, v. 25, n. 39, p. 8815–8824, 2005. ISSN 02706474. Disponível em: <<https://doi.org/10.1523/JNEUROSCI.0816-05.2005>>.

SANTELLO, M.; BIANCHI, M.; GABICCINI, M.; RICCIARDI, E.; SALVIETTI, G.; PRATTICIZZO, D.; ERNST, M.; MOSCATELLI, A.; JÖRNTELL, H.; KAPPERS, A. M.; KYRIAKOPOULOS, K.; ALBU-SCHÄFFER, A.; CASTELLINI, C.; BICCHI, A. Hand synergies: Integration of robotics and neuroscience for understanding the control of biological and artificial hands. *Physics of Life Reviews*, Elsevier B.V., v. 17, p. 1–23, 2016. ISSN 15710645. Disponível em: <<http://dx.doi.org/10.1016/j.plrev.2016.02.001>>.

SEDOV, A.; DEVET'YAROV, D.; SEMENOVA, Y.; ZAV'YALOVA, V.; USHAKOV, V.; MEDVEDNIK, R.; UBLINSKII, M.; AKHADOV, T.; SEMENOVA, N. fMRI Studies of the Dynamics of Human Brain Reactions on Execution of Voluntary Movements. *Neuroscience and Behavioral Physiology*, v. 46, n. 9, 2016. ISSN 1573899X.

SHAKEEL, A.; NAVID, M. S.; ANWAR, M. N.; MAZHAR, S.; JOCHUMSEN, M.; NIAZI, I. K. A review of techniques for detection of movement intention using movement-related cortical potentials. *Computational and Mathematical Methods in Medicine*, v. 2015, 2015. ISSN 17486718.

TAYLOR, R. L. American association for the advancement of science. *Journal of Clinical Endocrinology and Metabolism*, v. 10, n. 10, p. 1361–1362, 1950. ISSN 19457197. Disponível em: <<https://doi.org/10.1210/jcem-10-10-1361>>.

THOMAS, T. M.; CANDREA, D. N.; FIFER, M. S.; McMULLEN, D. P.; ANDERSON, W. S.; THAKOR, N. V.; CRONE, N. E. Decoding native cortical representations for flexion and extension at upper limb joints using electrocorticography. *IEEE Transactions on Neural Systems and Rehabilitation Engineering*, IEEE, v. 27, n. 2, p. 293–303, 2019. ISSN 15344320. Disponível em: <<https://doi.org/10.1109/TNSRE.2019.2891362>>.

Udhaya Kumar, S.; Hannah Inbarani, H. PSO-based feature selection and neighborhood rough set-based classification for BCI multiclass motor imagery task. *Neural Computing and Applications*, Springer London, v. 28, n. 11, p. 3239–3258, 2017. ISSN 09410643. Disponível em: <<https://doi.org/10.1007/s00521-016-2236-5>>.

- VALYEAR, K. F.; FREY, S. H. Human posterior parietal cortex mediates hand-specific planning. *NeuroImage*, Elsevier Inc., v. 114, p. 226–238, 2015. ISSN 10959572. Disponível em: <<http://dx.doi.org/10.1016/j.neuroimage.2015.03.058>>.
- VULLIEMOZ, S.; RODIONOV, R.; CARMICHAEL, D. W.; THORNTON, R.; GUYE, M.; LHATOO, S. D.; MICHEL, C. M.; DUNCAN, J. S.; LEMIEUX, L. Continuous EEG source imaging enhances analysis of EEG-fMRI in focal epilepsy. *NeuroImage*, Elsevier Inc., v. 49, n. 4, p. 3219–3229, 2010. ISSN 10538119. Disponível em: <<http://dx.doi.org/10.1016/j.neuroimage.2009.11.055>>.
- WANG, G.; REN, D. Effect of brain-to-skull conductivity ratio on EEG source localization accuracy. *BioMed Research International*, v. 2013, 2013. ISSN 23146133.
- WODLINGER, B.; DOWNEY, J. E.; TYLER-KABARA, E. C.; SCHWARTZ, A. B.; BONINGER, M. L.; COLLINGER, J. L. Ten-dimensional anthropomorphic arm control in a human brain-machine interface: Difficulties, solutions, and limitations. *Journal of Neural Engineering*, IOP Publishing, v. 12, n. 1, 2015. ISSN 17412552.
- WODLINGER, B.; DOWNEY, J. E.; TYLER-KABARA, E. C.; SCHWARTZ, A. B.; BONINGER, M. L.; COLLINGER, J. L. Ten-dimensional anthropomorphic arm control in a human brain-machine interface: Difficulties, solutions, and limitations. *Journal of Neural Engineering*, IOP Publishing, v. 12, n. 1, 2015. ISSN 17412552.
- YOSHIMURA, N.; TSUDA, H.; KAWASE, T.; KAMBARA, H.; KOIKE, Y. Decoding finger movement in humans using synergy of EEG cortical current signals. *Scientific Reports*, Springer US, v. 7, n. 1, p. 1–11, 2017. ISSN 20452322. Disponível em: <<http://dx.doi.org/10.1038/s41598-017-09770-5>>.